Phycological Research

Phycological Research 2025 doi: 10.1111/pre.70001

Diversity of Amphidomataceae (Dinophyceae) in the Black Sea, including description of *Amphidoma pontica* sp. nov.

Urban Tillmann,[1]* **Nina Dzhembekova**,[2] **Oana Vlas**,[3] **Bernd Krock**,[1] **Laura Boicenco**[3] **and Fuat Dursun**[4]

[1]Alfred Wegener Institut-Helmholtz Zentrum für Polar- und Meeresforschung, Ökologische Chemie, Bremerhaven, Germany, [2]Institute of Oceanology "Fridtjof Nansen" – Bulgarian Academy of Sciences, Varna, Bulgaria, [3]National Institute for Marine Research and Development "Grigore Antipa", Constanța, Romania and [4]Institute of Marine Sciences and Management, Istanbul University, Istanbul, Turkey

SUMMARY

The dinoflagellate family Amphidomataceae includes the genera *Azadinium* and *Amphidoma*, several species of which are known producers of lipophilic toxins known as azaspiracids (AZAs). However, the diversity, abundance, and distribution of this important group of nanoplanktonic dinoflagellates in the Black Sea remain poorly understood. To address this knowledge gap, Amphidomataceae were specifically investigated during a PHYCOB research cruise in the western Black Sea in September 2021. The study employed live microscopy observations on board, electron microscopy of field-collected samples, quantitative assessments of abundance and distribution in preserved samples, and the establishment of clonal strains. Amphidomataceae species were detected at all stations, with abundances ranging from 1.2 to 13.0×10^3 cells per liter. However, no AZAs were detected in any of the field samples. Light microscopy and subsequent SEM analyses revealed a high diversity of species. Field-sample-SEM-documented records included *Azadinium trinitatum*, *Az. spinosum*, *Az. luciferelloides*, an undescribed *Azadinium* species, *Amphidoma languida*, and an undescribed species of *Amphidoma*. Additionally, two clonal strains were successfully established and are newly described here as *Amphidoma pontica*. This new species closely resembles *Am. languida* and *Am. fulgens*, but is distinguished by the absence of contact between the distalmost apical plate (6′) and the distalmost precingular plate (6″). Molecular phylogenetic analysis based on concatenated ribosomal markers supports its classification as a distinct species. Neither of the *Am. pontica* strains produced detectable levels of AZAs. This study significantly contributes to a foundational assessment of the species diversity, distribution, and potential toxicity of Amphidomataceae in the Black Sea.

Key words: *Azadinium*, azaspiracids, diversity, electron microscopy, new species, taxonomy.

INTRODUCTION

The Black Sea is one of the world's most peculiar regional seas, largely isolated from the global ocean, characterized by low salinity (about 17–18 in the surface layer), strong vertical stratification, and euxinic conditions below depths of 150–200 m (Bakan & Büyükgüngör 2000). These features create challenging physiological conditions for its inhabitants and make Black Sea marine ecosystems highly sensitive to anthropogenic pressure (Zaitsev & Mamaev 1997; Bakan & Büyükgüngör 2000). Indeed, human impact has led to significant transformations of the Black Sea ecosystem in the past (Akoglu *et al*. 2014). Eutrophication, plankton blooms, and changes in species composition with an increase in dinoflagellate proportions, have been among the major threats to the health of its ecosystem (Zaitsev 1992; Moncheva *et al*. 2001; Nesterova *et al*. 2008). Despite improvements since the mid-1990s (Kideys 2002), the ecological state remains unstable, and plankton communities, as an indicator of marine environmental status, need to be monitored (Moncheva *et al*. 2019).

Indeed, red tides caused by different microalgal species have been observed in Black Sea waters even before the period of intense eutrophication, dating back to the 1920s (reviewed in Ryabushko 2003b). A total of 79 microalgal species have been considered potentially harmful, with 49 listed as potentially toxic (Ryabushko 2003a,b), though the toxigenic status of some species has changed over time. Furthermore, in some genera containing both toxigenic and non-toxigenic species, precise determination of species identity by light microscopy is challenging, if not impossible, due to resolution limitations and high intra-genus morphological similarity. Thus, the application of advanced identification techniques (e.g. scanning electron microscopy, molecular methods) is crucial for accurate species identification, revealing higher taxonomic diversity than previously reported (Baytut *et al*. 2013; Dzhembekova *et al*. 2017).

Marine amphidomatacean dinoflagellates are an example of arduous taxonomic delineation due to their small size and subtle morphological differences among species (Tillmann 2018a). The family encompasses the genera *Azadinium* Elbrächter & Tillmann and *Amphidoma* Stein, both of which attracted special attention due to the capability of some species to produce azaspiracids (AZAs), a group of lipophilic marine biotoxins associated with severe gastrointestinal human intoxications

*To whom correspondence should be addressed.
Email: urban.tillmann@awi.de
Received 6 May 2025; accepted 19 June 2025.

(Twiner *et al*. 2008). The increased scientific interest in the family, following the discovery of their toxigenic potential (Tillmann *et al*. 2009), has rapidly enhanced knowledge about Amphidomataceae diversity and distribution. A total of 17 species have been described within the genus *Azadinium* (Tillmann *et al*. 2009, 2010, 2011, 2012b, 2014a, 2020; Nézan *et al*. 2012; Luo *et al*. 2013, 2017; Percopo *et al*. 2013; Salas *et al*. 2021; Kuwata *et al*. 2023), and seven new species have been added to *Amphidoma* (Tillmann *et al*. 2012a, 2018b; Kuwata *et al*. 2024b), based in most cases on combined morphological (light microscopy and scanning electron microscopy) and molecular analyses. Despite challenges in species identification and limited knowledge of the biogeography of certain species, Amphidomataceae are now recognized to have a cosmopolitan distribution (Tillmann 2018a).

In the Black Sea, the family Amphidomataceae, represented by *Amphidoma languida* Tillmann, Salas & Elbrächter and *Azadinium spinosum* Elbrächter & Tillmann, has recently been added (but without documentation) to the updated list of dinoflagellate species based on single records from unpublished data (Krakhmalny *et al*. 2018). In addition, four more *Azadinium* species (*Az. concinnum* Tillmann & Nézan, *Az. dexteroporum* Percopo & Zingone, *Az. poporum* Tillmann & Elbrächter, and *Az. trinitatum* Tillmann & Nézan) have been detected using a metabarcoding approach (Dzhembekova *et al*. 2017, 2022; Zhang *et al*. 2020). Although no azaspiracids have been detected in plankton or shellfish samples from the Black Sea so far, considering the limited targeted investigations of this group of phycotoxins (Dzhembekova *et al*. 2022; Peteva *et al*. 2023) and the scarce data on Amphidomataceae in the area, it is essential to examine the regional species diversity, distribution, and toxicity of the family.

During the PHYCOB research cruise in September 2021 in the western part of the Black Sea, a targeted investigation of Amphidomataceae was conducted. Field water samples were microscopically analyzed for Amphidomataceae species and AZAs, and cultured strains of Amphidomataceae isolates were established. A new *Amphidoma* species was examined in detail regarding its morphology, phylogeny, and AZA production potential.

MATERIALS AND METHODS

Sampling

Samples were collected during the PHYCOB research cruise in September 2021 in the western Black Sea aboard the Turkish R/V TÜBITAK MARMARA. Water samples were taken with a Niskin bottle sampler and used to qualitatively check the plankton community for the presence of Amphidomataceae. Therefore, water from three depths (surface (3 m), 10 m, and thermocline) was pooled, and 1 L of this composite sample was gently concentrated by gravity filtration using 5 μm pore size polycarbonate filters. The concentrate was then observed using an inverted microscope (Axiovert 200 M; Zeiss; Jena, Germany) equipped with epifluorescence and differential interference contrast optics. Living cells of interest were documented on board at 630× magnification by single frame micrographs extracted from video records using a digital video camera (Gryphax; Jenoptik; Jena, Germany) at full-HD resolution.

Another 1 L aliquot of the pooled water sample was likewise concentrated and fixed with formaldehyde (1% final concentration) for later analyses using scanning electron microscopy (SEM).

Temperature profiles were measured using a CTD (SBE; SeaBird; Washington, DC, USA), equipped with a factory-calibrated Sea-Bird SBE 3F temperature sensor and SBE 4C conductivity sensor. The system was deployed at each station during the cruise, recording high-resolution data throughout the water column.

Amphidomataceae field sample cell counts

Identification and cell counts of water samples collected from Niskin bottles attached to a SeaBird CTD Rosette was conducted using an inverted microscope (IX73; Olympus; Tokyo, Japan), in Uthermöhl chambers (Moncheva & Parr 2010). One liter samples each were collected from three depths corresponding to the surface, thermocline, and deep chlorophyll maximum layers, and were preserved with 20 mL of 37% formaldehyde. In the laboratory, the samples were concentrated to approximately 30 mL using the sedimentation method which involved settling and removing the supernatant in two stages, performed biweekly (Moncheva & Parr 2010). The sample was then homogenized, and a 1 mL aliquot sample was thoroughly analyzed under the inverted microscope. For species identification, published taxonomic keys (Schiller 1937; Kisselew 1950; Tomas 1997) and online databases (World Register of Marine Species, Nordic Microalgae, AlgaeBase) were used as references. Cell counts included all planktonic protists in the nano- and micro size class regardless of their trophic status, but did not include ciliates and the giant protist species *Noctiluca scintillans*. Specifically, various cell types of Amphidomataceae with distinct shapes and sizes were all classified under the single category of 'Amphidomataceae'. The individual cell biovolume (μm^3) was determined by approximating the cell shape of each species to the most similar regular solid, with calculations based on the respective formulas routinely used in the laboratory, according to MISIS project intercalibration exercise (Moncheva *et al*. 2014). Cell biovolume (μm^3) was then converted to wet weight (ng) following Moncheva *et al*. (2014). Using the primary data obtained, abundance (cells L^{-1}) and wet weight ($\mu g\ L^{-1}$) were calculated.

The plots of the total and average *Amphidomataceae* abundance as well as the distribution of temperature by depths, were generated using Ocean Data View (ODV). Spatial interpolation was performed using the DIVA (Data-Interpolating Variational Analysis) gridded data style, a finite-element approach that accounts for both data distribution and coastline geometry to produce smooth gridded fields. Default settings were applied, with the correlation length automatically determined (Schlitzer 2023).

The average density (AvD) and biomass (AvB) in the water column were calculated using the trapezoidal rule. This method approximates the area under the curve of density vs. depth, then normalizes it by the total depth range. The rule involves summing the values at each interval (e.g. d1 and d2, d2 and d3, …, dn-1 and dn), where the first and last

values are averaged ((d1 + d2)/2), and the result is multiplied by the depth interval (e.g. z2 – z1, zn-1 – zn). The entire sum is then divided by the total depth range, calculated as the maximum depth value (zn) minus the minimum depth value (z1) as follows

$$\frac{\left[\frac{d1+d2}{2}\cdot(z2-z1)+\frac{d2+d3}{2}\cdot(z3-z2)+\ldots.+\frac{dn-1+dn}{2}\cdot(zn-zn-1)\right]}{zn-z1}$$

AZA analysis of field samples

Water samples for AZA analyses were collected from all 23 stations. A total of 8 to 9.5 L of pooled water from three depths (surface (3 m), 10 m, and thermocline) was screened with 20 μm gauze and subsequently filtered through 5 μm pore size polycarbonate filters under a gentle vacuum (<200 mbar). The material retained on the filters was extracted by repeated rinsing with methanol until complete discoloration of the filters. The resulting methanolic extracts were transferred to centrifugation filters (Millipore Ultrafree; Eschborn, Germany) and filtered through a 0.45 μm cut-off membrane by centrifugation for 30 s at 3220 × *g*. The final filtrates were adjusted to a volume of 300 μL and transferred into analytical glass vials and stored at −20 °C for subsequent liquid chromatography-tandem mass spectrometry (LC–MS/MS) analysis.

Reagents, e.g., formic acid (90%, p.a.), acetic acid (96%, p.a.) and ammonium formate (98%, p.a.) (Merck; Darmstadt, Germany), used in the analysis were of analytical grade. The solvents, methanol and acetonitrile, were of high-performance liquid chromatography (HPLC) grade (Merck; Darmstadt, Germany) and deionized water was obtained from a purification system (Milli Q, Millipore). Mass spectral experiments were performed to survey a wide array of AZAs using an analytical system consisting of a triple quadrupole mass spectrometer equipped with a TurboSpray interface (Sciex-4000 Q Trap; Sciex; Darmstadt, Germany), coupled to a liquid chromatograph (LC) (model 1100; Agilent; Waldbronn, Germany). The LC equipment included a solvent reservoir, in-line degasser (G1379A), binary pump (G1311A), refrigerated autosampler (G1329A/G1330B), and temperature-controlled column oven (G1316A).

Separation of AZAs (5 μL sample injection volume) was performed by reversed-phase chromatography. The analytical column (50 × 2 mm) was packed with 3 μm C8 phase (Hypersil BDS 120 Å; Phenomenex; Aschaffenburg, Germany) and maintained at 20 °C. The flow rate was 0.2 mL min^{-1}, and gradient elution was performed with two eluents, where eluent 'A' was water and 'B' was acetonitrile/water (95:5 v/v), both containing 2.0 mM ammonium formate and 50 mM formic acid. Initial conditions were 8 min column equilibration with 30% B, followed by a linear gradient to 100% B in 8 min and isocratic elution until 18 min with 100% B then returning to initial conditions until 21 min (total run time: 29 min).

AZAs were screened in one period (0–18 min) with curtain gas: 10 psi, CAD: medium, ion spray voltage: 5500 V, temperature: ambient, nebulizer gas: 10 psi, auxiliary gas: off, interface heater: on, declustering potential: 100 V, entrance potential: 10 V, exit potential: 30 V. Selected reaction monitoring (SRM) experiments were carried out in positive ion mode by selecting the following transitions shown in Table S1. AZAs were calibrated against an external standard solution of AZA-1 (100 pg μL^{-1}) (certified reference material (CRM) programme of the IMB-NRC, Halifax, Canada) and estimated as AZA-1 equivalents. The limit of detection was defined as signal-to-noise ratio (S/N) = 3 estimated by a one-point calibration with a 100 pg μL^{-1}standard solution of AZA-1. Data acquisition and processing was performed with the Analyst Software (version 1.5; Sciex).

Strain isolation, growth, and sampling

Cells of Amphidomataceae were isolated on board using a micropipette and a stereomicroscope (Olympus SZH; Olympus; Hamburg, Germany) with a maximum of 64 × magnification and dark field illumination which allow detection and isolation of such small cells. Single cells were transferred into individual wells of 96-well tissue culture plates (TPP; Trasadingen, Switzerland) containing 250 μL of medium prepared from 0.2 μm sterile-filtered medium (Keller *et al*. 1987) diluted with seawater from the sampling location at a ratio of 1:10. The original K-medium recipe was slightly modified by replacing the organic phosphorus source by 3.62 μM Na_2HPO_4. Plates were incubated at room temperature (ca. 20 °C) using artificial light of 30–50 μmol m^{-2} s^{-1} and a 16:8 h light:dark photocycle. Cells from these wells were re-isolated and washed until unialgal cultures were obtained. Established strains were transferred to 24-well tissue culture plates, each well containing 2 mL medium. Unfortunately, most of the successfully isolated strains did not survive transportation back to the home laboratory in Germany. However, two strains (denoted as BS 6-F6 and BS 6-F9, both isolated from station 18) could finally be established and grown in batch cultures in 65 mL polystyrene cell culture flasks at 20 °C under a photon flux density of 30–50 μmol m^{-2} s^{-1} and a 16:8 h light:dark photocycle in a controlled environment growth chamber (Model MIR 252; Sanyo Biomedical; Etten-Leur, The Netherlands). The culture medium consisted of sterile filtered (0.2 μm VacuCap filters; Pall Corporation, Port Washington, NY, USA) natural North Sea water diluted to a salinity of about 20, enriched with nutrient according to the modified K-medium described above.

For toxin analysis, strains were grown under the standard culture conditions described above. For each harvest, cell density was determined by settling Lugol's fixed samples and counting >400 cells under an inverted microscope in order to calculate toxin cell quota. Densely grown strains (ranging from ca. 1.8–6.0 × 10^3 cells mL^{-1}) were harvested by centrifugation (5810R; Eppendorf; Hamburg, Germany) at 3220 × *g* for 10 min of 50 mL subsamples. The cell pellet was resuspended, transferred to a microtube, centrifuged again (5415; Eppendorf; 16 000 × *g*, 5 min), and stored frozen (−20 °C) until use. For strain BS 6-F9, growth and harvest procedures were repeated two times to yield higher biomass (in total 2.41 × 10^6 cells) for increased sensitivity of the toxin detection method.

For DNA harvest, cells of both strains were collected by centrifugation (5810R; Eppendorf) in 50 mL centrifugation tubes at 3220 × *g* for 10 min. Cell pellets were transferred with 0.5 mL lysis buffer (SL1, provided by the NucleoSpin Soil DNA extraction Kit; Macherey-Nagel; Düren, Germany) to

1 mL microtubes and stored frozen (−20 °C) for subsequent DNA extraction. Genomic DNA was extracted following the manufacturers' instructions of the NucleoSpin Soil DNA extraction Kit (Macherey-Nagel; Düren, Germany) with an additional cell disruption step within the beat tubes; the samples were shaken in a FastPrep FP120 cell disrupter (Qbiogene; Carlsbad, CA, USA) for 45 s and another 30 s at a speed of 4.0 m s^{-1}.

Microscopical analyses of strains

Light microscopy (LM) observation of cells of both strains was carried out with an inverted microscope (Axiovert 200 M; Zeiss; Jena, Germany) or a compound microscope (Axioskop 2; Zeiss; Jena, Germany). The shape and location of the nucleus was determined after staining of formalin-fixed cells with 4′,6-diamidino-2-phenylindole (DAPI, 0.1 μg mL^{-1} final concentration) for 10 min. Cell length and width were measured at 1000 × microscopic magnification using Zeiss Axiovision software (Zeiss; Jena, Germany) and photographs of formaldehyde fixed cells (1% final concentration). Photographs were taken with an Axiocam MRc5 digital camera (Zeiss; Jena, Germany).

For scanning electron microscopy (SEM), cells of both strains were collected by centrifugation (5810R, Eppendorf; 3220 × *g* for 10 min) from 15 mL of the strain. The supernatant was removed, and the cell pellet was re-suspended in 60% ethanol prepared in a 2-mL microtube with seawater (final salinity ca. 13) at 4 °C for 1 h in order to strip off the outer cell membrane. Cells were further collected by centrifugation (5415R, Eppendorf; 16 000 × *g* for 5 min), resuspended and fixed in a 60:40 mixture of deionized water and seawater (final salinity ca. 13) with the addition of formaldehyde (1% final concentration), and stored at 4 °C for 3 h. In addition, selected formaldehyde-fixed field samples (plankton concentrate) were examined by SEM as well. Cells from all samples were collected on polycarbonate filters (25 mm Ø, 3 μm pore size, Millipore Merck; Darmstadt, Germany) in a filter funnel, in which all subsequent washing and dehydration steps were carried out. A total of eight washing steps (2 mL MilliQ-deionized water each) were followed by a dehydration series in ethanol (30, 50, 70, 80, 95, and 100%; 10 min each). Filters were finally dehydrated with hexamethyldisilazane (HMDS), first in 1:1 HMDS:EtOH and then twice in 100% HMDS, and then stored in a desiccator under gentle vacuum. Finally, filters were mounted on stubs, sputter-coated (SC500; Emscope; Ashford, UK) with gold–palladium, and viewed by SEM at 10 kV (FEG 200; FEI Quanta; Eindhoven, the Netherlands). Micrographs were presented on a black background using Photoshop 6.0 (Adobe Systems; San Jose, CA, USA).

Sequencing of strains and phylogenetic analyses

To determine the small subunit ribosomal DNA (SSU rDNA), large subunit ribosomal DNA (LSU rDNA), and internal transcribed spacer (ITS) sequences of BS 6-F6 and BS 6-F9 strains, the following forward and reverse primers were used: 1F and 1528R (Tillmann *et al.* 2009), ITSA and ITSB (Sato *et al.* 2011), and D1R and D2C (Scholin *et al.* 1994). For SSU rDNA amplification, each PCR reaction was performed in 50 μL reaction volume using 25 μL HotStarTaq Master Mix Kit (QIAGEN; Hilden, Germany), 2 μL of each primer (0.4 μM), and ~ 15 ng of DNA. The PCR amplification included an initial denaturation step for 15 min at 95 °C, followed by 30 cycles of 1 min at 94 °C, 1 min at 54 °C and 1 min at 72 °C, with a final extension for 5 min at 72 °C. For ITS and LSU rDNA amplification, each reaction was performed in 20 μL reaction volume using AccuPower® HotStart PCR PreMix (Bioneer Corporation; Daejeon, Republic of Korea). The reaction mix contained 0.5 μL of each primer (0.25 μM), and ~ 15 ng of DNA. The PCR amplification included an initial denaturation step for 5 min at 94 °C, followed by 30 cycles of 30 s at 94 °C, 1 min at 55 °C and 1 min at 72 °C, with a final extension for 5 min at 72 °C. PCR products were purified and sequenced in both directions at Macrogen Europe (Amsterdam, The Nethelands). The sequences were manually edited using MEGA X (Kumar *et al.* 2018) and are available in GenBank (Clark *et al.* 2016) under the accession numbers listed in Table S2.

For phylogenetic analyses, sequences of Amphidomataceae representatives (*Amphidoma* and *Azadinium*) from different geographic locations as well as of *Prorocentrum pervagatum* Tillmann, Hoppenrath & Gottschling (used as an outgroup), were obtained from GenBank (Clark *et al.* 2016). The strains were selected based on the availability of their SSU rDNA, LSU rDNA, and ITS sequences, except for *Amphidoma parvula* Tillmann & Gottschling, for which no SSU sequence is available (Table S2). Sequence alignment was performed using MAFFT version 7 (Katoh *et al.* 2019) online program (http://mafft.cbrc.jp/alignment/server/) with default settings. The dataset used for phylogenetic analyses included SSU, ITS, and LSU alignments of 54 partial sequences, which were concatenated into a single file.

A phylogenetic tree was constructed using the maximum likelihood (ML) method in MEGA 12 (Kumar *et al.* 2024), with the best substitution model, the general time reversible (GTR) model (Nei & Kumar 2000), incorporating a discrete Gamma distribution (G) across five categories (parameter = 0.5375) and 63.56% evolutionarily invariant sites (I), as selected by the software based on the lowest Akaike information criterion (AIC) scores. Bootstrap support values for ML analyses were estimated using 1000 replicates.

Posterior probabilities of Bayesian inference (BI) were estimated using MrBayes v.3.2 (Ronquist *et al.* 2012). For BI, four Markov chain Monte Carlo (MCMC) chains were run for 1,000,000 generations, with sampling every 100 generations. The first 25% of burn-in trees were discarded. The substitution model used for BI analyses was GTR + I + G, selected based on the lowest AIC scores using MrModeltest2 (Nylander 2004).

The pairwise genetic distance between *Amphidoma* strains from the Black Sea (BS 6-F6 and BS 6-F9) and the strains of the other *Amphidoma* species used in the phylogenetic analyses was calculated with MEGA 12 (Kumar *et al.* 2024).

AZA analysis of strains

For azaspiracid (AZA) analysis of the strains BS 6-F6 and BS 6-F9, cell pellets of both strains were extracted with 500 μL

acetone and vortexed every 10 min during 1 h at room temperature. Homogenates were centrifuged at 3220 × *g* for 15 min. Supernatants were then transferred to a 0.45 μm pore-size spin-filter and centrifuged at 800 × *g* for 30 s, with the resulting filtrate adjusted with acetone to 500 μL and transferred into a liquid chromatography (LC) autosampler vial for liquid chromatography-tandem mass spectrometry (LC–MS/MS) analysis.

Selected reaction monitoring (SRM) experiments and data acquisition and processing were performed to survey a wide array of AZAs (Table S1) as described above for the field samples.

In order to test for putative novel AZAs, precursor ion experiments were performed with the characteristics AZA fragments *m/z* 348, *m/z* 350, *m/z* 360, *m/z* 362 and *m/z* 378 in the positive-ion mode from *m/z* 500 to 1000 under the following conditions; curtain gas: 10 psi, CAD: medium, ion spray voltage: 5500 V, temperature: ambient, nebulizer gas: 10 psi, auxiliary gas: off, interface heater: on, declustering potential: 100 V, entrance potential: 10 V, collision energy: 70 V, exit potential: 12 V.

RESULTS

Description of the new species

Both new strains of Amphidomataceae obtained in the present study were identified as a new species of *Amphidoma*. Both strains were identical in terms of morphology and plate pattern. Strain BS 6-F9 was selected to prepare the holotype and is described and depicted in detail below.

Amphidoma pontica Tillmann & Dzhembekova sp. nov.

Description: Small photosynthetic thecate Dinophyceae; cells 12.2 to 14.4 μm long and 9.4 to 11.9 μm wide; cingulum broad (c. 23% of cell length) and postmedian; epitheca conical dome shaped and ending in a small but distinctly pointed apical pore; hypotheca hemispherical with a narrow sulcus; tabulation formula: po, cp, X, 6′, 0a, 6″, 6C, 5S, 6‴, 2⁗; no contact of plates 6′ and 6″; a ventral pore located on the right anterior part of plate 1′; a large ventral depression on the tip of plate sa, and an antapical pore on plate 2⁗.

Holotype: SEM stub prepared from clonal strain BS 6-F9 (designated CEDiT2025H204), deposited at the Senckenberg Research Institute and Natural History Museum, Centre of Excellence for Dinophyte Taxonomy (Wilhelmshaven, Germany).

Reference Material: Formalin-fixed sample prepared from clonal strain BS 6-F9 (designated CEDiT2025RM205) deposited at the Senckenberg Research Institute and Natural History Museum, Centre of Excellence for Dinophyte Taxonomy (Wilhelmshaven, Germany).

Type locality: Black Sea (42°58.153′ N; 28°7.494′ E).

Habitat: Marine plankton.

Strain establishment: Sampled and isolated by U. Tillmann, September 2021.

Etymology: The epithet (Latin ponticus – referring to the Black Sea) indicates that this species was first observed in the Black Sea.

This taxonomic act has been registered in PhycoBank (http://phycobank.org/105393).

Detailed description

Cells of strain BS 6-F9 were small with a mean length of 13.5 ± 0.6 μm (min 12.2 – max 14.4, $n = 30$) and a mean width of 10.6 ± 0.7 μm (min 9.4 – max 11.9, $n = 30$). *Amphidoma pontica* was ovoid to slightly elliptical in outline (Fig. 1a–f). A single round pyrenoid was located in the episome (Fig. 1b). The episome itself was conical and dome-shaped with a distinctly pointed apical pore (Fig. 1c,f). It was slightly larger than the rounded or slightly flattened hyposome. The submedian cingulum was broad, incised and displaced by about half of the cingulum width (Fig. 1e). Cells were slightly compressed dorsoventrally (Fig. 1f). Cells sometimes possessed shining refractile inclusions at the posterior end of the hyposome (Fig. 1b–d). Thecal plates of *Am. pontica* were thin but clearly visible when shed by ecdysing cells (Fig. 1g). Cells divided in motile stage by desmoschisis (Fig. 1h). One large lobed chloroplast expanded the whole cell (Fig. 1i,j). A large, round nucleus was located in the hyposome or in the cingular plain (Fig. 1k–m). During cell division, the nucleus became ellipsoid (Fig. 1n) and elongated and then divided perpendicular to the cell axis (Fig. 1o).

In culture, cells of *Am. pontica* usually concentrated at the bottom of the observation chamber. They exhibited a conspicuous swimming behaviour. A generally very slow movement was irregularly interrupted by sudden jumps (Video S1 provided as Supplementary Material).

Due to its small size, the plate pattern was most easily resolved by electron microscopy (Figs 2–4). The plate formula of *Am. pontica* was po, cp, X, 6′, 0a, 6″, 6C, 5S, 6‴, 2⁗, and is schematically drawn in Fig. 5a–d.

Plates were smooth, but growth bands of thecal plates were occasionally faintly visible as striated rows running parallel to plate sutures (Fig. 2a–c). The dome-shaped epitheca terminated in the apical pore complex (APC; Fig. 2a–d), which was composed of a pore plate (po) covered by a cover plate (cp), and a small X (or canal) plate (Fig. 3f–h). The pore plate was teardrop-shaped (1.3 ± 0.1 μm in width and 1.8 ± 0.1 μm in length; $n = 16$) with a blunt ventral termination (Fig. 3h) and confined by a collar formed by edges of the apical plates. The collar was narrow and raised, and thus was distinct in LM (Fig. 1c,f). On the tapered ventral side of the pore plate, the collar was open and extended ventrally along the sutures of the first and sixth apical plate (Fig. 3a–g). In the center of po, a round pore (diameter 0.9 ± 0.1 μm; $n = 16$) emerged which was covered by a cover plate (cp). A small X-plate was located where the pore plate abutted the first apical plate and was most clearly visible in internal views (Fig. 3h). From the exterior, the X-plate had a characteristic three-dimensional structure with a finger-like protrusion connected to the apical cover plate (Fig. 3f,g).

There was a series of six apical plates around the APC (Figs 2f and 3a,b). The first apical plate was long, narrow, and slightly asymmetric in that its right suture to plate 6′ was slightly longer than the left suture to plate 2′ (Figs 2a,c–e and 3b–d). Moreover, on the left side of plate 1′ there was one long and straight suture with plate 1″, whereas the right side of plate 1′ was asymmetric and contacting two of the precingular plates, i.e. plates 6″ and 5″ (Fig. 3c,d). The other apical plates were rather small, of comparable size, and only about one-fifth the length of precingular plates (Figs 2a–d,f–h and 3a–c). Most of

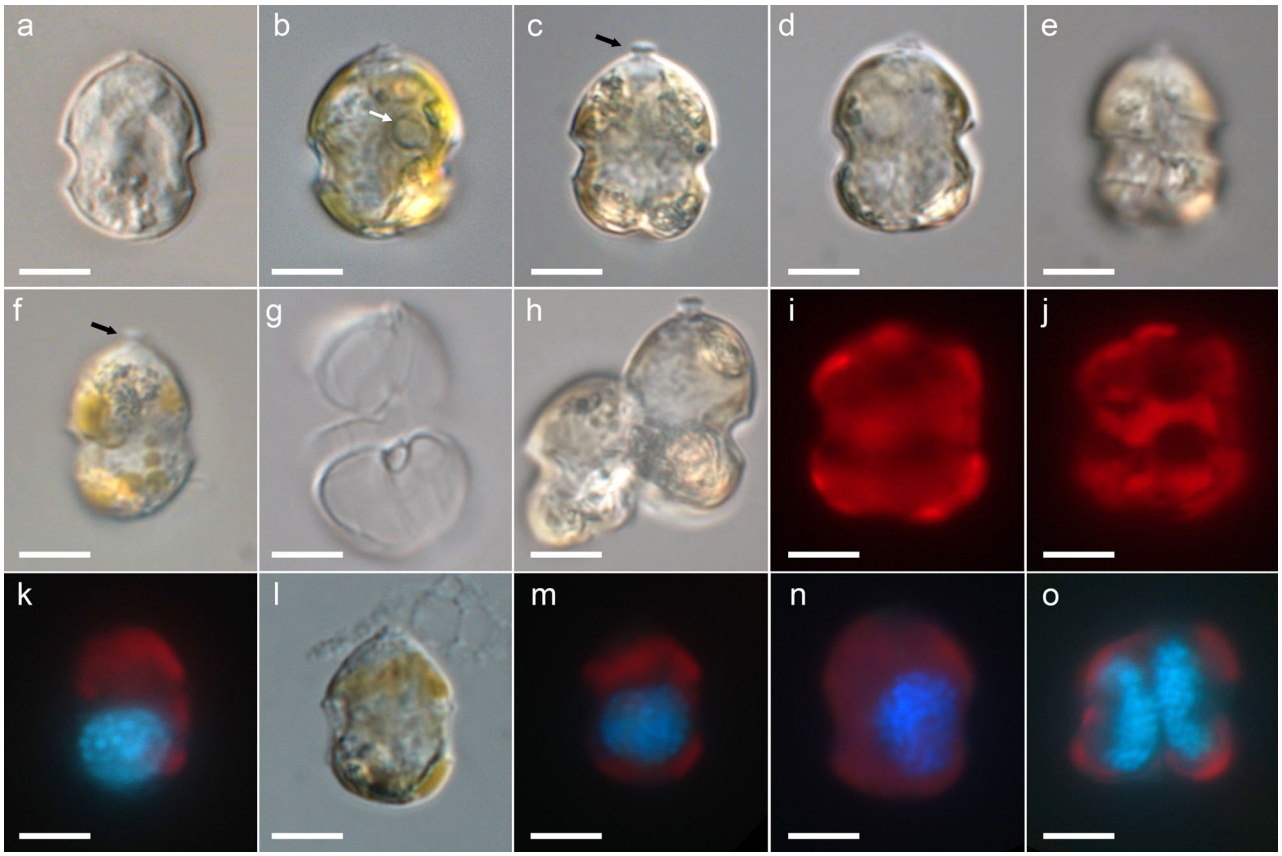

Figure 1. *Amphidoma pontica* sp. nov. (strain BS 6-F9). LM of formalin fixed cells (a, i–o) or live cells (b–h). (a–f) General size and shape of cells in dorsal/ventral view (a–e) or lateral view (f). Note the prominent apical pore complex (black arrow in c and f) and the pyrenoid (white arrow in b) in the episome. (g) Empty theca. (h) Late stage of cell division (desmoschisis). (i, j) Two different focal planes of a cell with blue light excitation showing the reticulate chloroplast. (k, l) The same cell stained with DAPI with UV light excitation (k) and in brightfield (l) to indicate shape, size and location of the nucleus (blue) and the chloroplast (red). (m–o) Other cells stained with DAPI with UV light excitation. (n) Cell in early stage of cell division, note the slightly elongated nucleus. (o) Late stage of nuclear division. Scale bars: 5 μm.

the lateral and dorsal apical plates were five-sided with precingular plates in contact with two apical plates. As a remarkable exception, plate 6′ was four-sided and in contact with plate 5″ only, as the contact between plates 6′ and 6″ was prevented by the shape of the first apical plate (Fig. 3a–d). Sutures between apical plates were marked by ridges which were part of plates 3′ and 5′ and by plates 2′ and 6′ (Fig. 3a–g). A ventral pore was present in apical position on the right side of plate 1′ (Fig. 3b,c, g,h) and was often at least partly hidden by the rim of plate 6′. This pore had a distinct rim with an outer diameter of 0.22 μm ± 0.03 μm ($n = 24$). Precingular plates were of comparable size, except for plate 6″, which was significantly shorter and narrower (Figs 2a,c–e and 3a–c).

The hypotheca was composed of six postcingular and two antapical plates. Among postcingular plates, plates 2‴ to 5‴ were comparably wide, whereas the ventrally located plates 1‴ and 6‴ were narrower (Figs 2 and 4a). The two antapical plates were unequal in size, with plate 2⁗ being about double the size of the first antapical plate (Fig. 4a). Plate 2⁗ bore a larger antapical pore (0.31 ± 0.04 μm in diameter, $n = 23$) close to the meeting point of plate 2⁗ with postcingular plates 3‴ and 4‴. This antapical pore was surrounded by a broad rim and in fact was a sunken field of several small pores (Fig. 4h).

The cingulum was broad (23 ± 1% of total cell length in SEM measurements, $n = 10$), incised and with small lists towards both the epi- and hypotheca (Fig. 2a–h). There were six cingular plates (Fig. 4b,f). Five were of comparable size, but the right cingular plate C6 was distinctly narrower. All cingular plate sutures were nearly aligned with the respective sutures of precingular plates (Fig. 2a–h). The sulcus (Figs 2a,c–e and 4c–e,g) was deeply concave, narrow but slightly wider posteriorly and reached approximately to the middle of the hypotheca. The sulcal plates were difficult to resolve because of the internal vaulted structure of the flagellar pore region. Five sulcal plates could be identified. The large anterior sulcal plate (sa) was asymmetric and partly invaded the epitheca (Figs 2a,c–e and 4d). On the anterior tip of plate sa there was a large (0.60 ± 0.06 μm in diameter, $n = 35$) and conspicuous roundish depression bordered by a rim, i.e. the ventral depression. Two small plates, namely a median sulcal (sm) and a right sulcal (sd) plate, formed the

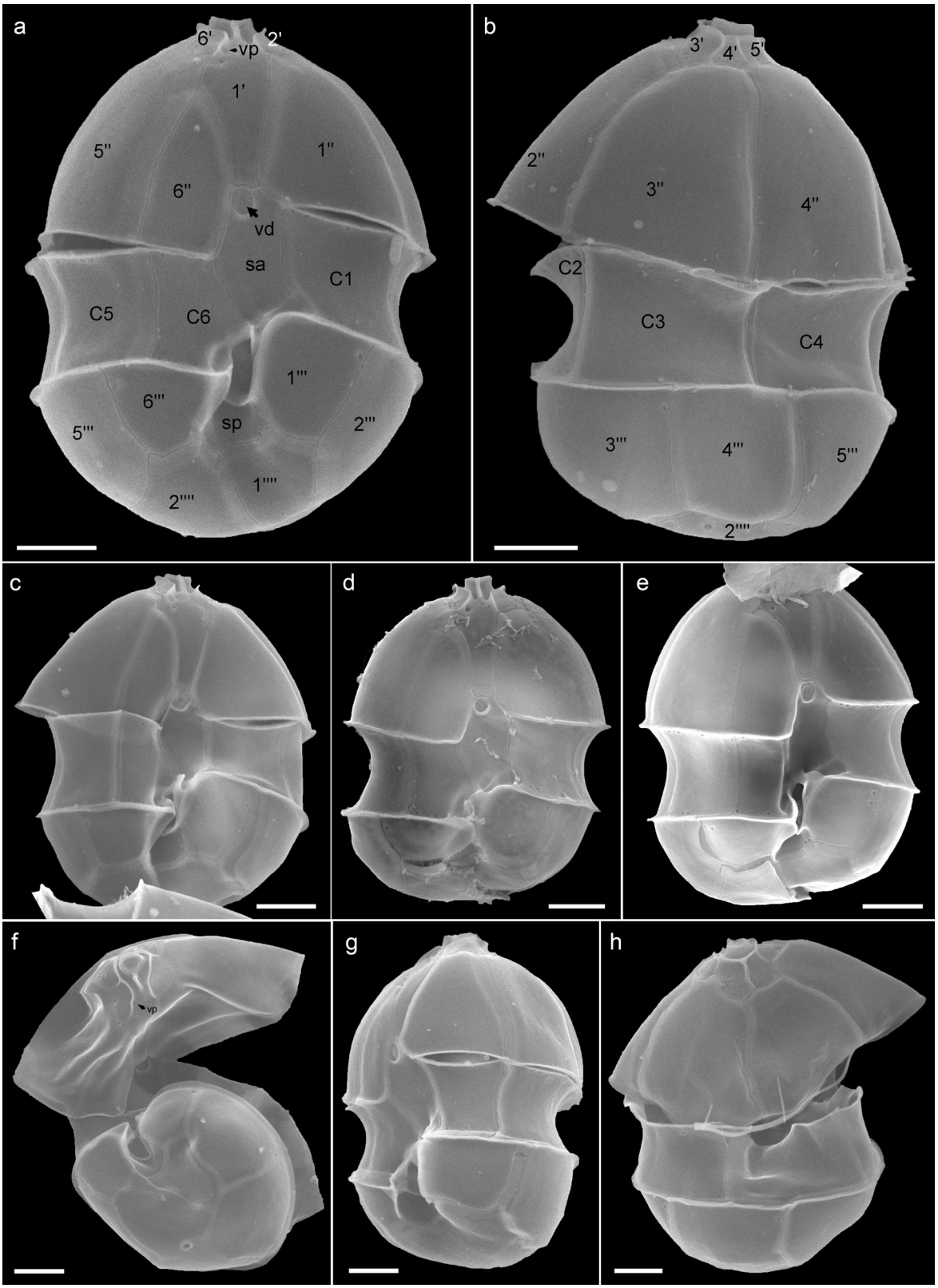

Figure 2. *Amphidoma pontica* sp. nov. (strain BS 6-F9). SEM micrographs of different cells in ventral view (a, c–f), dorsal view (b, h), or left-lateral view (g). 1′–6′, apical plates; 1″–6″, precingular plates; C1–C6, cingular plates; sa, anterior sulcal plate; sp., posterior sulcal plate; vd, ventral depression; vp, ventral pore. Scale bars: 2 μm.

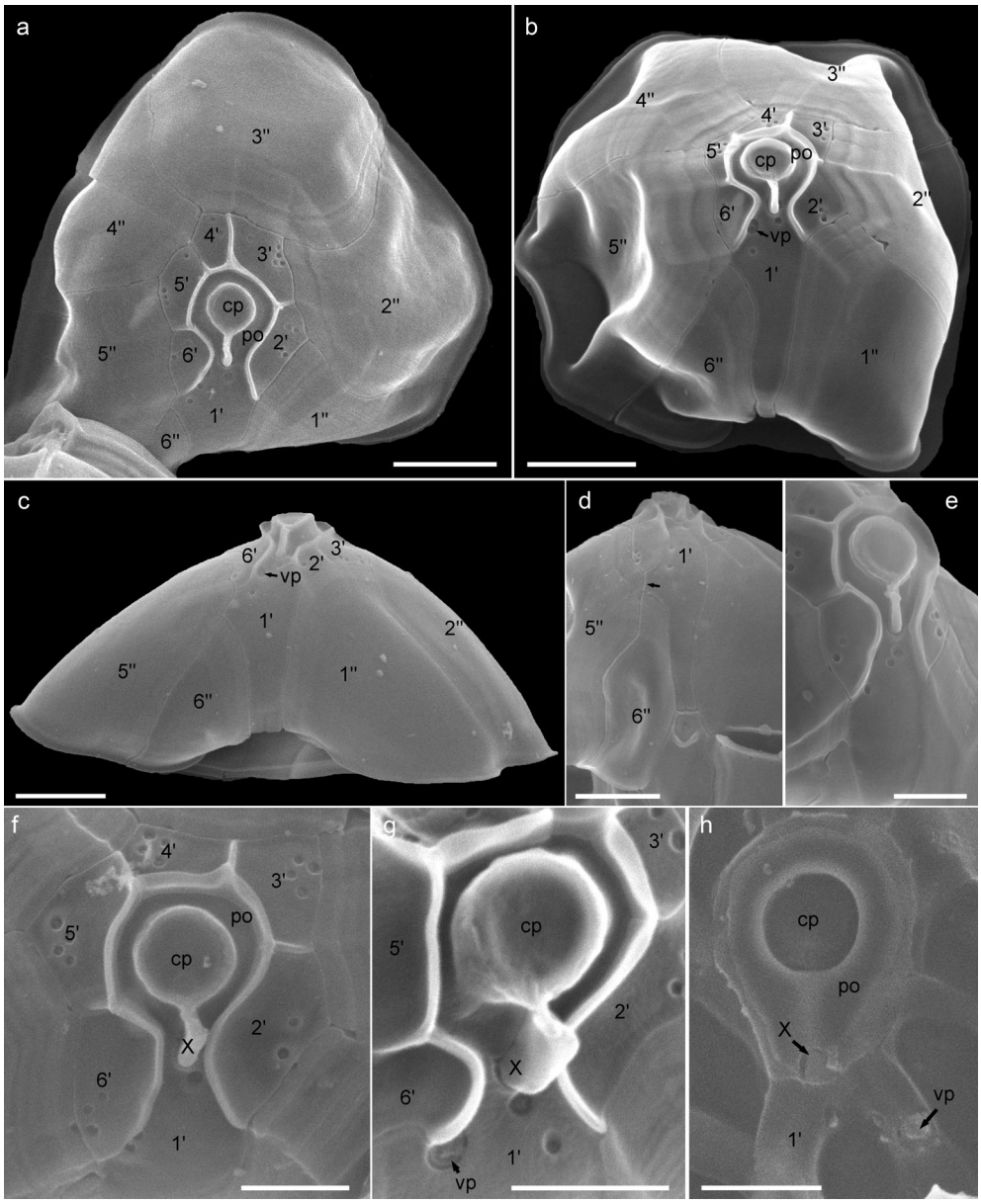

Figure 3. *Amphidoma pontica* sp. nov. (strain BS 6-F9). SEM micrographs of different thecae. (a–c) Epithecal plates in apical view (a, b) or ventral view (c). (d) Detailed ventral view of the first apical plate, note the suture of plate 1′ and 5″ (arrow). (e–h) Detailed view of the apical pore complex in external (e–g) or internal view (h). cp, cover plate; po, pore plate; X, X-plate; 1′–6′, apical plates; 1″–6″, precingular plates; vp, ventral pore. Scale bars: 2 μm (a–d) or 1 μm (e–h).

inverted part of the sulcus (Fig. 4f,g). A left sulcal plate (ss) ran horizontally from C1 to C6, thereby separating the posterior sulcal plate (sp) from the other sulcal plates. In its median and right part, this plate was very narrow and therefore difficult to resolve and to discern from the parallel running anterior ridge of the sp plate (Fig. 4c–e). The posterior sulcal plate was deeply concave, wider than long and was laterally bordered towards the last postcingular plate by a distinct sulcal list (Fig. 4c–e).

Apical plates had small pores of slightly variable size ranging from 0.08 to 0.13 μm in diameter (mean 0.10 ± 0.03 μm; $n = 20$). The number of pores varied between one and five per plate with three or four pores per plate being most common. On the first apical plate, these few small pores were present in addition to the distinctively larger ventral pore. In contrast to the apical plates, all precingular plates were consistently free of pores. On the cingular plates there were irregular short rows or clusters of few pores close to the sutures towards the epi- and the hypotheca (Fig. 2a–h). Postcingular plates usually had one pore per plate located close to the suture, but the dorsally located plate 4‴ was free of pores (Figs 2b and 4a). On both antapical plates there was either no or just one small pore present.

The plate pattern shown in Fig. 5 was standard; however, some variation occurred in culture. Common (but not quantified) variation involved deviations in the number

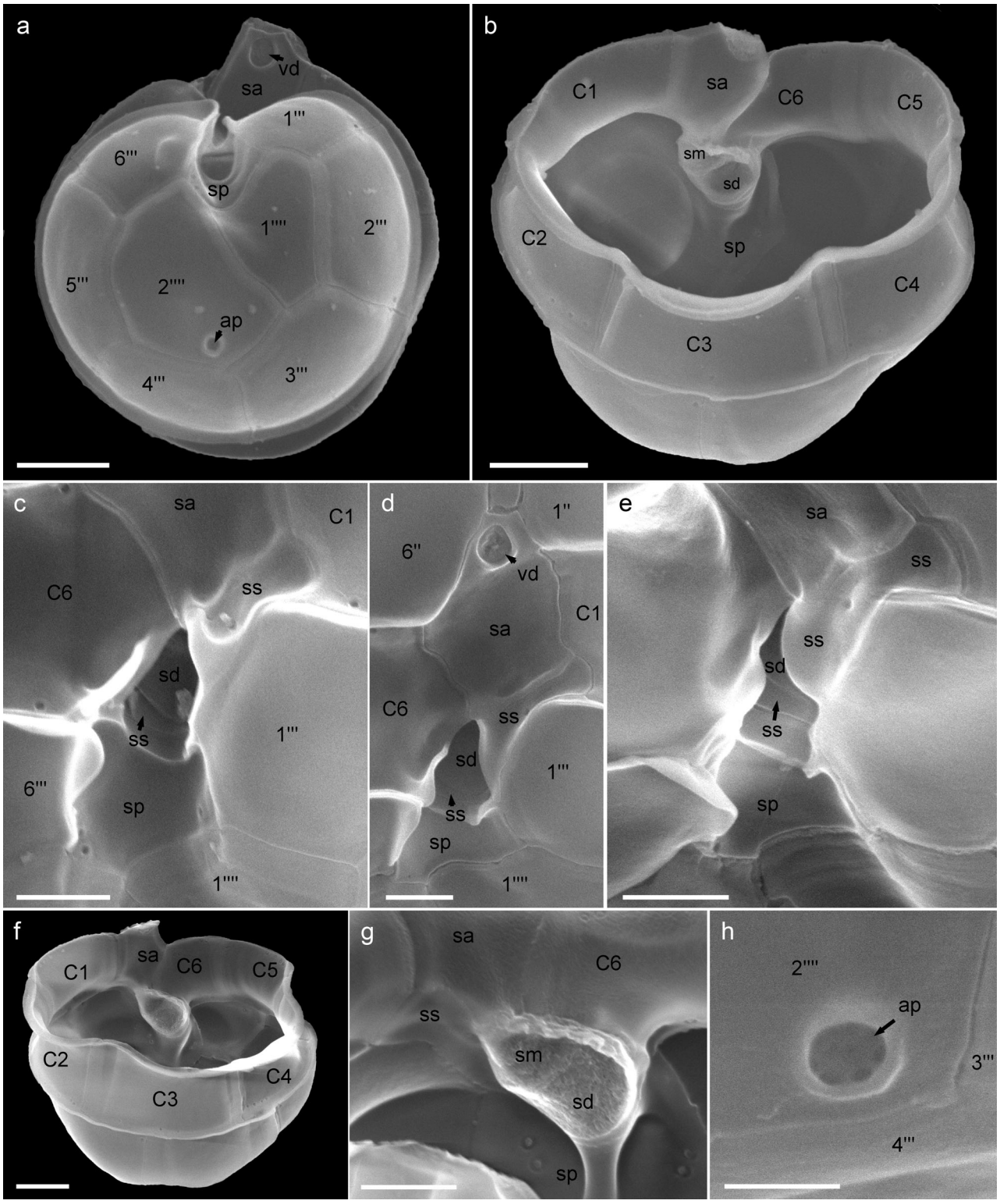

Figure 4. *Amphidoma pontica* sp. nov. (strain BS 6-F9). SEM micrographs of different thecae. (a, b) Hypothecal plates in antapical view (a) or apical-dorsal view (b). (c–e) Sulcal plates in external view. (f, g) The same hypotheca in low magnification (f) showing cingular plates, and in high magnification (g) for an internal view of sulcal plates. (h) Detailed view of the antapical pore on plate 2⁗. C1–C6, cingular plates; sa, anterior sulcal plate; sp, posterior sulcal plate; ss, left sulcal plate; sm, median sulcal plate; sd, right sulcal plate; 1‴–6‴, postcingular plates; 1⁗ and 2⁗, antapical plates; ap, antapical pore. Scale bars: 2 μm (a, b, f) or 1 μm (c–e, g) or 0.5 μm (h).

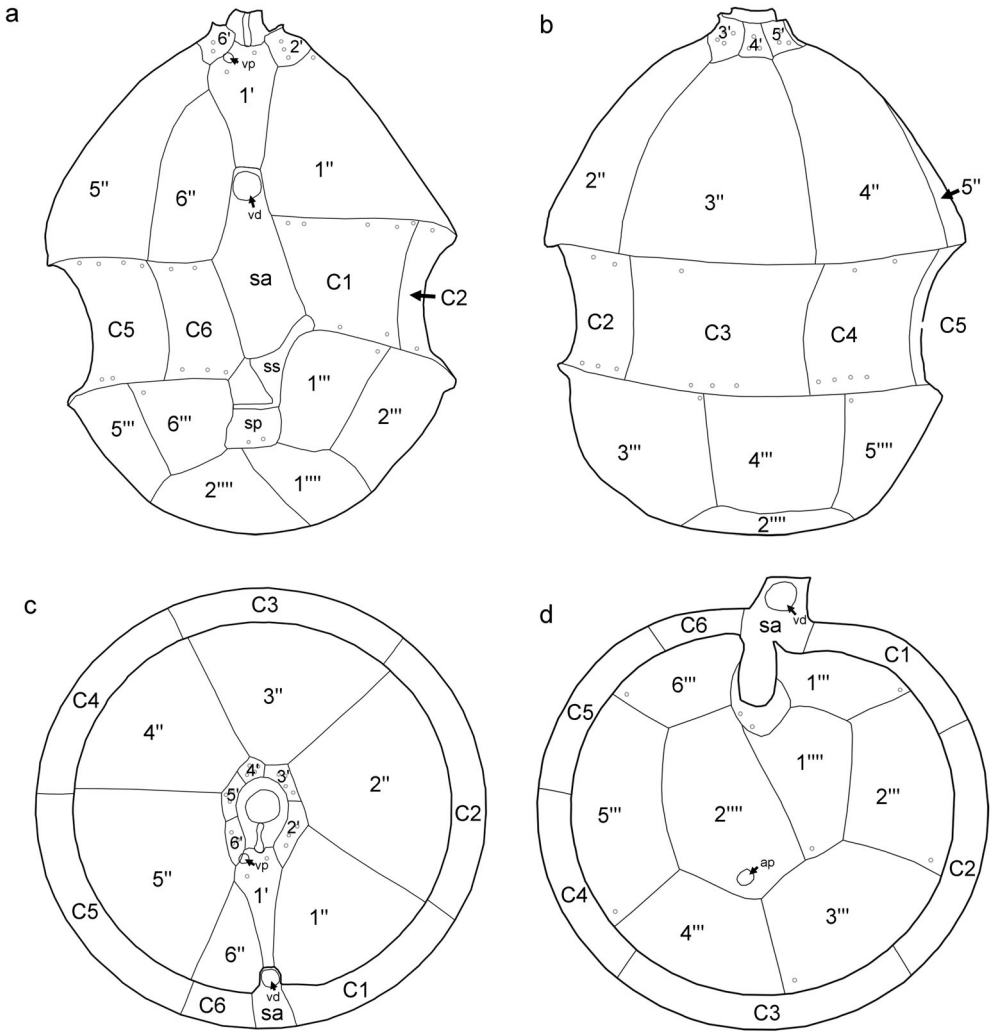

Figure 5. *Amphidoma pontica*. Diagrammatic illustration of thecal plates and position of thecal pores. (a) Ventral view; (b) Dorsal view; (c) Apical view; (d) Antapical view.

of apical or postcingular plates reflecting either the fusion of two plates or the splitting of one plate into two (Fig. S1a–f).

Sequence data and phylogeny

Both strains of *Amphidoma pontica* (BS 6-F6 and BS 6-F9) shared identical SSU, ITS, and LSU rDNA sequences. The SSU + ITS + LSU alignment used for phylogenetic analyses included 54 nucleotide sequences, was 3150 bp long, and contained 645 parsimony-informative sites. The best-scoring ML tree is shown in Figure 6. The genus *Amphidoma* formed a well-supported monophyletic clade within the Amphidomataceae group (ML100%, BI 1.00). Within the *Amphidoma* clade, the new *Am. pontica* formed a separate branch (ML 100%, BI 1.00), which clustered with a well-supported group (ML 99%, BI 1.00) formed by *Am. languida* and *Am. fulgens* K.Kuwata, K.Takahashi, W.M.Lum, G.Benico & Iwataki. *Amphidoma parvula* emerged as a distinct lineage in the *Amphidoma* clade.

The genetic distances between *Am. pontica* and the analyzed strains of other *Amphidoma* species were high based on the ITS region (16 sequences, 639 positions), ranging from 0.169 to 0.228 (Table S3). The distances were lower based on the LSU region (16 sequences, 779 positions) and particularly on the SSU region (15 sequences, 1697 positions), with ranges of 0.068–0.130 and 0.009–0.012, respectively (Tables S4 and S5). *Am. pontica* exhibited the lowest genetic distance to *Am. fulgens* in all analyzed regions.

DNA sequences of *Am. pontica* determined in this study are available in GenBank with accession numbers of PV290483 (SSU), OQ383680 (ITS), and OQ383717 (LSU) for BS 6-F6 strain, and PV290484 (SSU), OQ383681 (ITS), and OQ383717 (LSU) for BS 6-F9 strain (Table S2).

Amphidomataceae diversity in field samples

On board light microscopy using live samples revealed the presence of Amphidomataceae throughout the sampling area (Fig. 7a–s). Classification was based on size, shape, and the

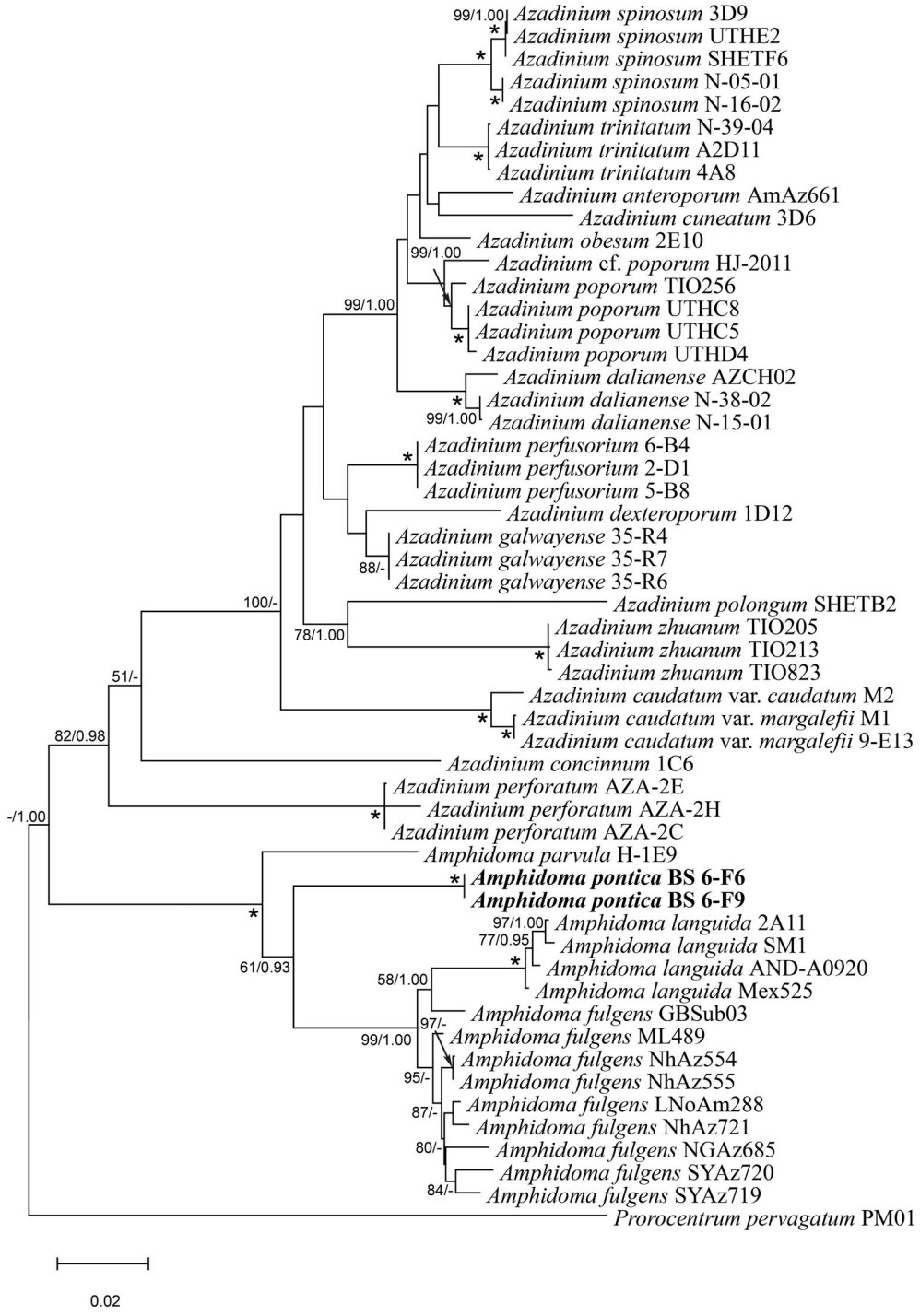

Figure 6. Phylogeny of Amphidomataceae species inferred from concatenated SSU, ITS, and LSU rDNA sequences using maximum likelihood (ML) method. *Prorocentrum pervagatum* was used as an outgroup. The tree is drawn to scale, with branch lengths measured in the number of nucleotide substitutions per site. Node labels represent bootstrap values from the ML method and posterior probabilities from Bayesian inference (ML/BI); only bootstrap values >50% and posterior probabilities >0.9 are shown. The sequences of *Am. pontica* are indicated in bold. * denotes maximal support, defined as 100%/1.00.

presence of a wide and distinct cingulum and of a distinctly pointed apex. LM indicated the presence of a number of different species, but with LM, no attempt was made to identify cells to the species level. With SEM analysis of the concentrated formaldehyde-fixed bottle sample of selected PHYCOB stations, a number of amphidomatacean species were identified (Figs 8–10). Specimens of the new species *Am. pontica* were observed in the field samples (Fig. 8a–m),

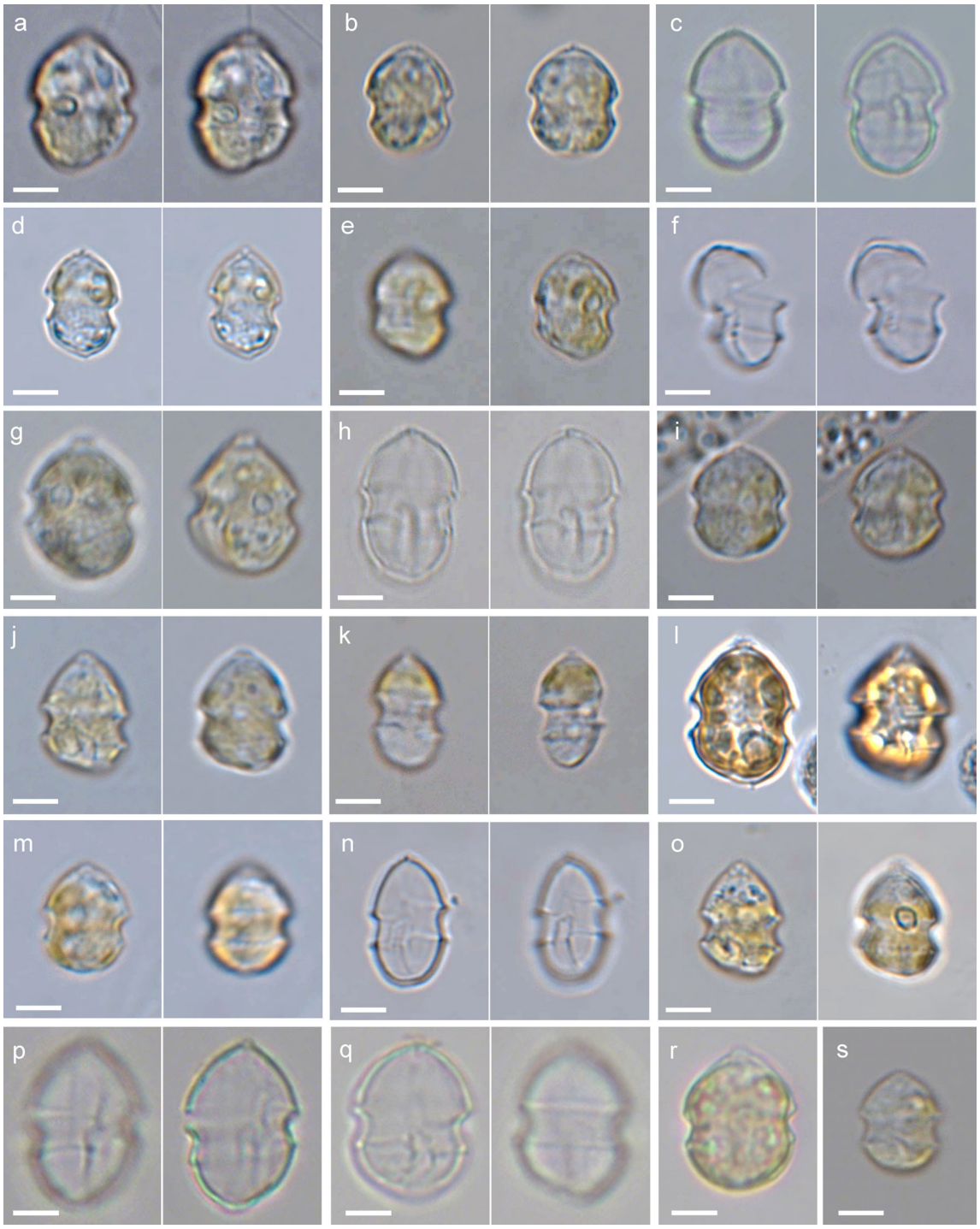

Figure 7. Diversity of Amphidomataceae in the western Black Sea as recorded during the PHYCOB survey by live onboard light microscopy. Two different focal planes (a–q) or single micrographs (r, s) of unidentified *Azadinium* and/or *Amphidoma* sp. cells or empty theca. Scale bars: 5 μm.

and these conformed to the morphological description of both isolated strains. Additional species of Amphidomataceae were identified as follows: A number of cells/fragments were identified as *Az. trinitatum* (Figs 9a–c, S2a–l) based on shape, position of the ventral pore on the left side of the pore plate, the presence of a small antapical spine, and the presence of small and narrow lateral apical plates. Other cells with a ventral pore located in the middle of the first apical plate close to the suture of plate 1″ were identified as *Az. spinosum* (Figs 9d–j, S3a,b). The antapical spine of these specimen was rather short. There were both specimens with a distinct rim around the pore plate (described as characteristic for *Az.*

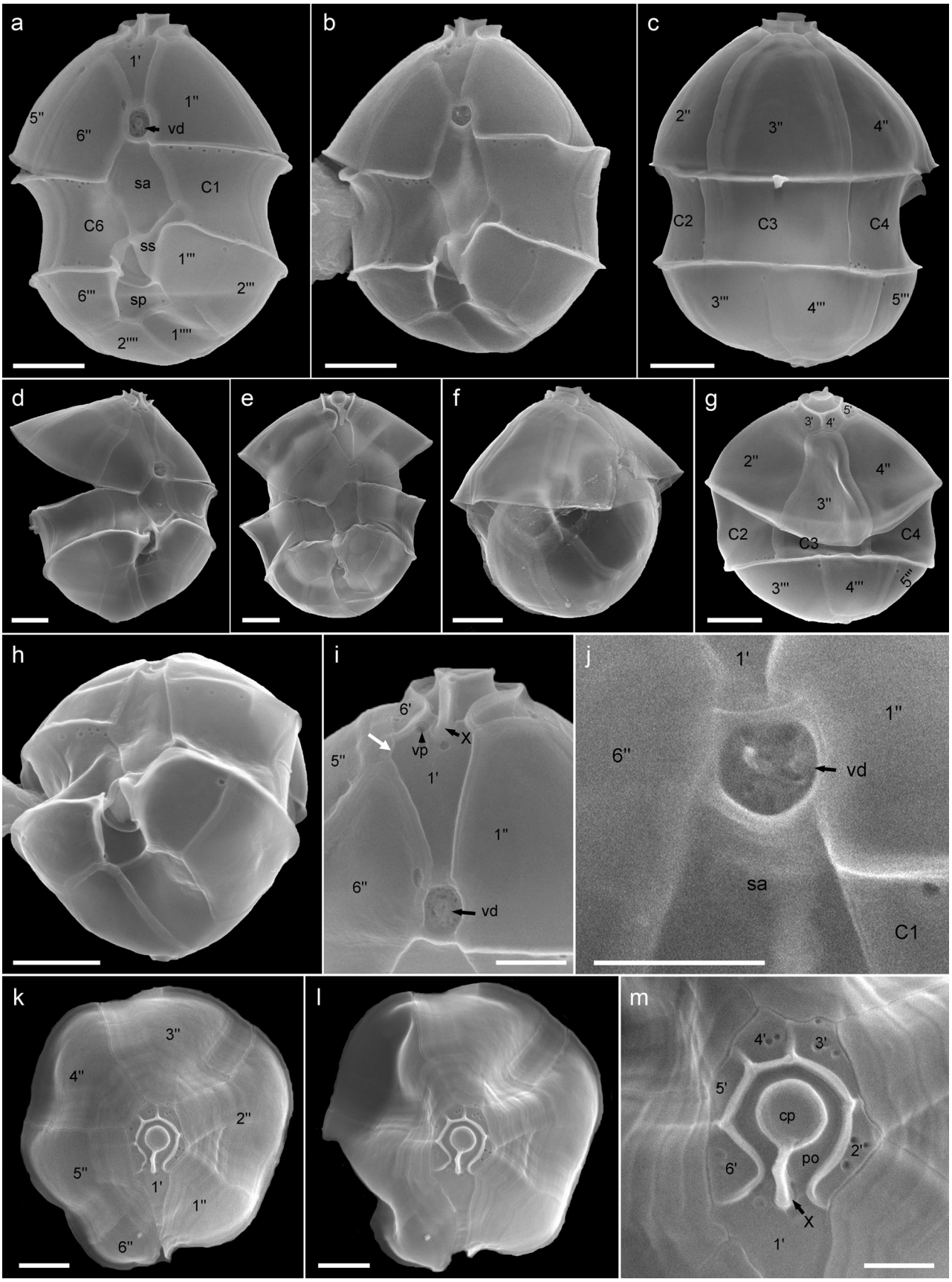

Figure 8. Legend on next page.

spinosum ribotype A) (Fig. 9d–e), and cells clearly lacking such a rim (Fig. 9g–i) which is described as characteristic for *Az. spinosum* ribotype B (Tillmann *et al.* 2018a). One comparable cell (Fig. 9j) with a similar short antapical spine had a slightly more oval cell shape and a distinct position of the ventral pore located in an elongated lateral bulge of the first apical plate, and thus remained unspecified. A few cells conformed to the species description of *Am. languida* (Figs 10a–c and S3c–f). They had a small ventral depression (Fig. 10a), a broad contact of plates 6′ and 6″, and one or few pores on the precingular plates (Figs 10b,c and S3d–f).

One cell of a yet undescribed *Azadinium* was observed (*Azadinium* sp. 1, Fig. 10d,e). In the ventral view there was a very broad first apical plate with a ventral pore located on the suture of plates 1′ and 4′ (Fig. 10e). It was not possible to clearly assign other thecae to this *Azadinium* sp. 1, but one with a distinctly large and pentagonal plate 2a (Fig. 10f) potentially represented a dorsal view of this undescribed species.

One theca fragment was observed where the epithecal plate arrangement and the ventral pore position conform with *Az. luciferelloides* Tillmann & Akselman (Fig. 10g, h). Moreover, shape and arrangement of epithecal plates in dorsal view of two other cells agreed with *Az. luciferelloides* as well, and both cells had a pentagonal plate 2a (Fig. 10i, j).

Finally, there were a number of cells which represented another yet undescribed species of Amphidomataceae (Figs 10k–m, S3g–n). These cells had an amphidomatacean APC with the characteristically shaped three-dimensional X-plate (Fig. 10k, m), but there were five large apical plates of about the same length as precingular plates, with two of them in symmetric dorsal position. Cells had small pores around the pore plate and distinct short rows of pores bordered anteriorly by a ridge on the apical plates. On the second antapical plate there was a field of >20 small pores (Figs 10l, S3h,i,k,l). For one apical view of a cell with a similar appearance the presence of six apical plates was observed (Fig. S3n).

Field sample abundance and distribution of Amphidomataceae

Quantitative LM analyses of the preserved samples revealed the presence of Amphidomataceae species in all 23 stations (Fig. 11a), contributing on average 8.6 ± 7.6% (min: 0.3%; max: 37.2%) to total abundance and 3.3 ± 4.5% (min: 0.1%; max: 26.8%) to total wet weight. Abundances exhibited spatial and vertical variability, ranging from 0.16×10^3 cells L^{-1} to peaks exceeding 13.0×10^3 cells L^{-1} (e.g. Station 9, deeper layer). Corresponding wet weight values varied between 0.05 and 5.62 μg L^{-1}. Amphidomatacean peaks were generally confined to surface or near-surface warmer layers (around 20–22.5 °C), consistent with stratified vertical profiles. In contrast, lower values were often detected in deeper and cooler layers (9–13 °C). The maximum abundance and biomass were recorded at an intermediate temperature of approximately 20.3 °C at Station 9 (Fig. 11a,b).

The distribution map of Amphidomataceae average abundance reveals distinct hotspots (Fig. 12). Station 9 (Tuzla) stands out as the most prominent area of elevated abundance and wet weight, with mean values of 7.59×10^3 cells L^{-1} and 2.04 μg L^{-1}. Other hotspots include the offshore station 12 (Shabla) and the coastal stations 8 (Midia), 10 (Durankulak), and 16 (Kaliakra), where also consistently high average abundance values ($3–4 \times 10^3$ cells L^{-1}) were observed. In contrast, the lowest averages were recorded at Stations 5 (Tuzla, offshore waters), 7 (Sinoe, coastal waters), and 17 (Varna, coastal waters), where abundance remained below 1×10^3 cells L^{-1} (Fig. 11a).

Azaspiracids

Selected reaction monitoring (SRM) analysis of all field samples was negative for the screened AZAs (Table S1) with a limit of detection (S/N = 3) of between 16.5 and 19.6 pg L^{-1} seawater (depending on the filtered water volume).

None of the screened azaspiracids was detected in strains BS 6-F6 and BS 6-F9, with a LOD of 0.33 fg $cell^{-1}$ for strain BS 6-F6 (cell pellet of 1.82×10^6 cells) and 0.25 fg $cell^{-1}$ for strain BS 6-F9 (cell pellet of 2.41×10^6 cells), respectively.

In order to test for putative novel AZAs, precursor ion experiments with the typical AZA fragments (*m/z* 348, *m/z* 350, *m/z* 360, *m/z* 362 and *m/z* 378) were performed but were negative for both strains. As precursor ion experiments are less sensitive, the LOD for this search for novel AZA was 10.74 fg $cell^{-1}$ and 8.09 fg $cell^{-1}$ for strain BS 6-F6 and BS 6-F9, respectively.

DISCUSSION

Diversity and abundance of Amphidomataceae in the Black Sea

Using four approaches, (1) light-microscopy on-board documentation of living Amphidomataceae cells, (2) electron microscopy documentation of Amphidomataceae in field

Figure 8. *Amphidoma pontica* sp. nov., SEM micrographs of different cells and thecae as observed in field samples. Cells in ventral view (a, b, e), in dorsal view (c, g), in right-lateral view (d) or in antapical-ventral view (h). (f) A cell, in which the epitheca has slipped over the hypotheca. (i) Detailed ventral view of the first apical plate, note the broad contact of plate 1′ and 5″ (white arrow). (j) Detailed view of the ventral depression at the anterior tip of plate sa. (k–m) Epithecal plates in apical view. The same theca is shown as two different snapshots to account for slight deformation of the theca during observation. (m) Detailed view of the apical pore complex of the same theca at higher magnification. 1′–6′, apical plates; 1″–6″, precingular plates; C1–C6, cingular plates; 1‴–6‴, postcingular plates; 1⁗ and 2⁗, antapical plates; sa, anterior sulcal plate; sp., posterior sulcal plate; ss, left sulcal plate; vd, ventral depression; vp, ventral pore; cp, cover plate; po, pore plate; X, X-plate. Scale bars: 2 μm (a–h, k, l) or 1 μm (i, j, m).

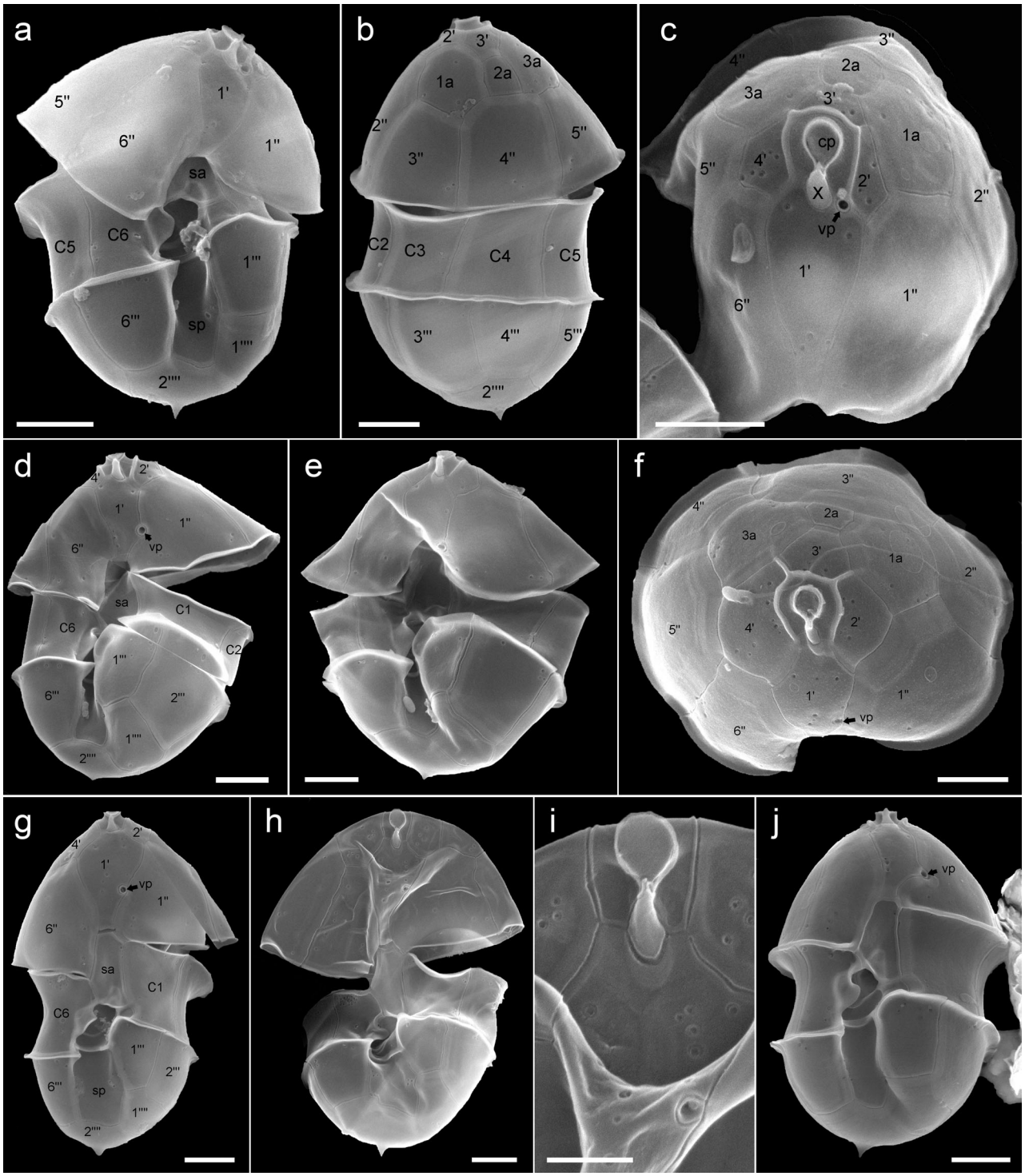

Figure 9. SEM of *Azadinium* cells observed in the Black Sea field sample. (a–c) *Azadinium trinitatum*, cells in ventral (a) and dorsal view (b). (c) Apical view showing the complete series of epithecal plates. (d–j) *Azadinium* cf. *spinosum*. Cells in dorsal view (d, e, g, h, j). (f) Details of epithecal plates in apical view. (i) Detailed ventral view of the apical pore complex and the first apical plate. Note that cells in d–f have a pronounced rim around the apical pore plate which is typical for *Az. spinosum* ribotype A, whereas cells in g–j lack such a rim, which is typical for *Az. spinosum* ribotype B. 1′–6′, apical plates; 1″–6″, precingular plates; C1–C6, cingular plates; 1‴–6‴, postcingular plates; 1⁗ and 2⁗, antapical plates; sa, anterior sulcal plate; sp., posterior sulcal plate; vp, ventral pore; cp, cover plate; X, X-plate. Scale bars: 2 μm.

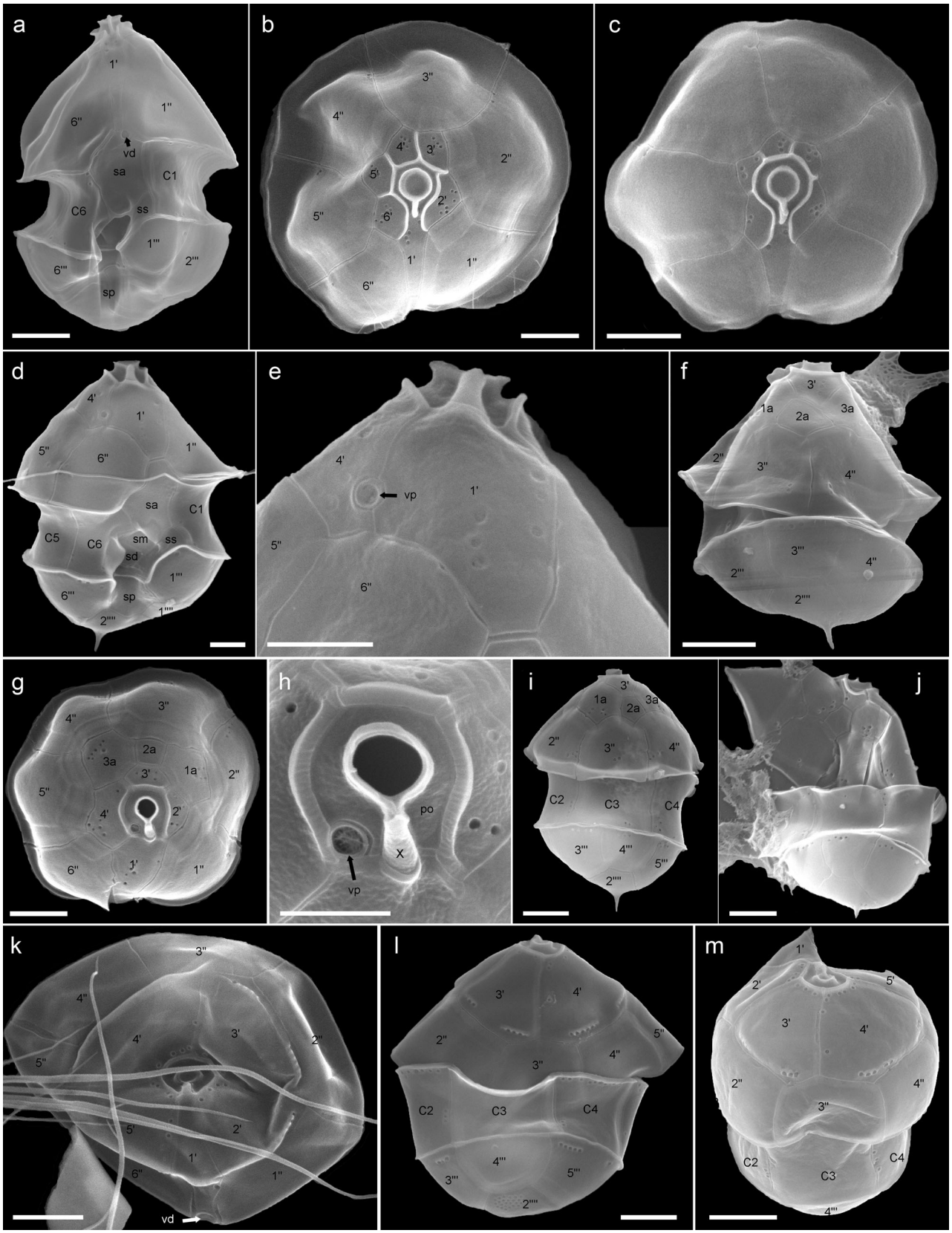

Figure 10. Legend on next page.

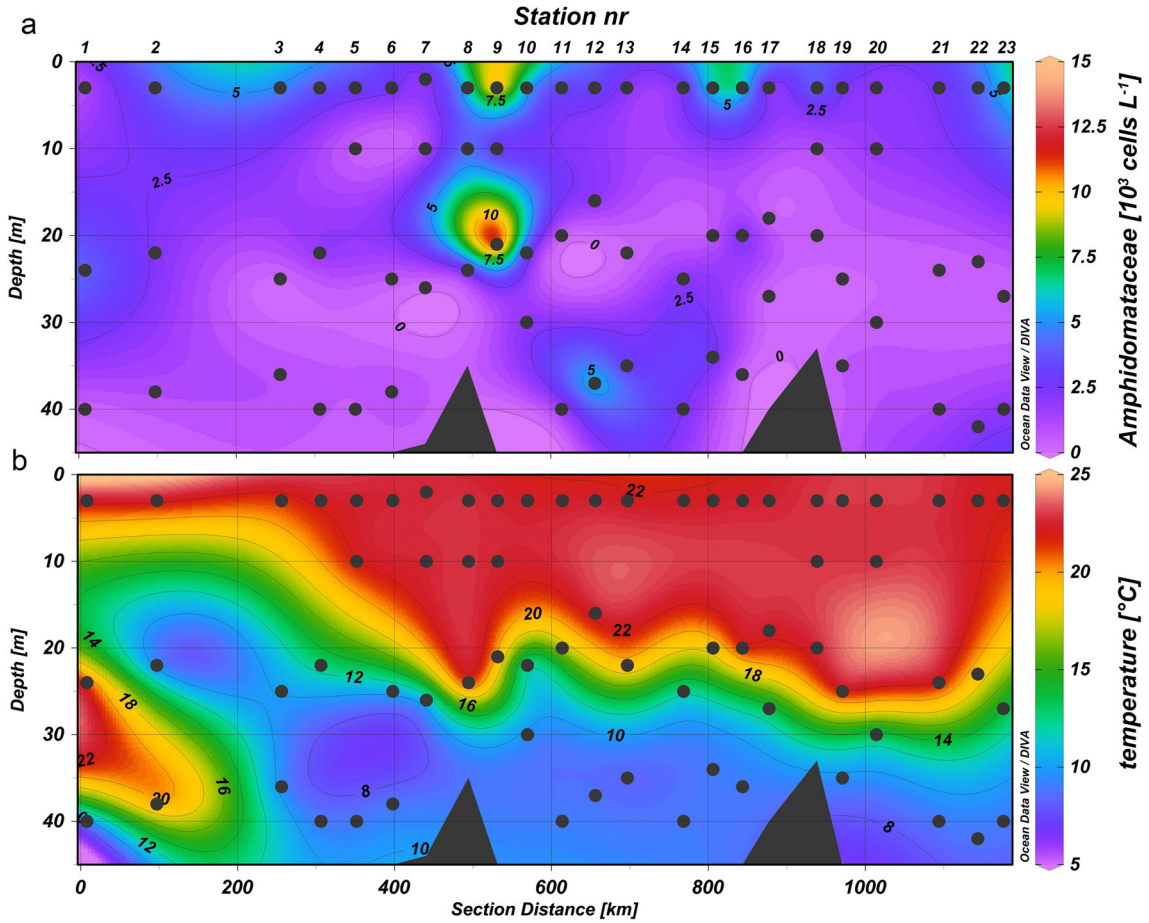

Figure 11. Distribution of (a) total Amphidomataceae abundance (10^3 cells L^{-1}) and (b) temperature (°C) by sampling depths along the Western Black Sea, from station 1 to 23. Thin lines in the plots represent contour lines of equal values, used to visualize the spatial distribution patterns across the sampled stations and depths. The position of the stations can be inferred from Fig. 12.

samples, (3) quantitative estimates of amphidomatacean abundance and distribution by analyzing fixed field samples; and (4) the description of a new species of *Amphidoma* based on two isolated strains, this paper makes a significant contribution to understanding the diversity and importance of this family of dinoflagellates in the Black Sea. This is particularly relevant because some species of Amphidomataceae produce toxins (Krock *et al*. 2019) and have caused massive problems for aquaculture in other regions, especially in the Atlantic off the coast of Ireland (Salas *et al*. 2011).

Live observations during the PHYCOB cruise clearly show that Amphidomataceae are present at all stations throughout the study area. Their quantitative distribution highlights a patchy pattern, likely shaped by local environmental conditions such as temperature, stratification and water column stability. Different cell shapes as seen under a light microscope indicate the presence of multiple species. However, a reliable species identification is not possible this way, as the diagnostic features of most Amphidomataceae species – except for *Azadinium caudatum* (Halldal) Nézan & Chomérat, which is distinguishable by its characteristic cell shape (Nézan

Figure 10. SEM of *Azadinium* and *Amphidoma* cells observed in the Black Sea field sample. (a–c) *Amphidoma languida*. (a) Cell in ventral view. (b, c) Apical view showing the complete series of epithecal plates. (d–f) *Azadinium* sp. 1. (d) Cell in ventral view. (e) High magnification view of the same cell as in (d) to emphasize the characteristic position of the ventral pore (vp). (f) Cell in dorsal view likely representing *Azadinium* sp. 1. (g–j) *Az. luciferelloides*. (g) Apical view showing the complete series of epithecal plates. (h) High magnification of the same cell as in (g) to illustrate the apical pore complex and the position of the ventral pore (vp). (i, j) Dorsal view of two cells likely representing *Az. luciferelloides*. (k–m) Cells of a yet undetermined *Amphidoma* sp. 1. (k) Apical view showing epithecal plates. (l) Cell in dorsal view. (m) Cell in dorsal/apical view. 1′–6′, apical plates; 1″–6″, precingular plates; C1–C6, cingular plates; 1‴–6‴, postcingular plates; 1⁗ and 2⁗, antapical plates; sa, anterior sulcal plate; sp., posterior sulcal plate; ss, left sulcal plate; sm; median sulcal plate; sd, right sulcal plate; vd, ventral depression; vp, ventral pore; po, pore plate; X, X-plate. Scale bars: 2 μm.

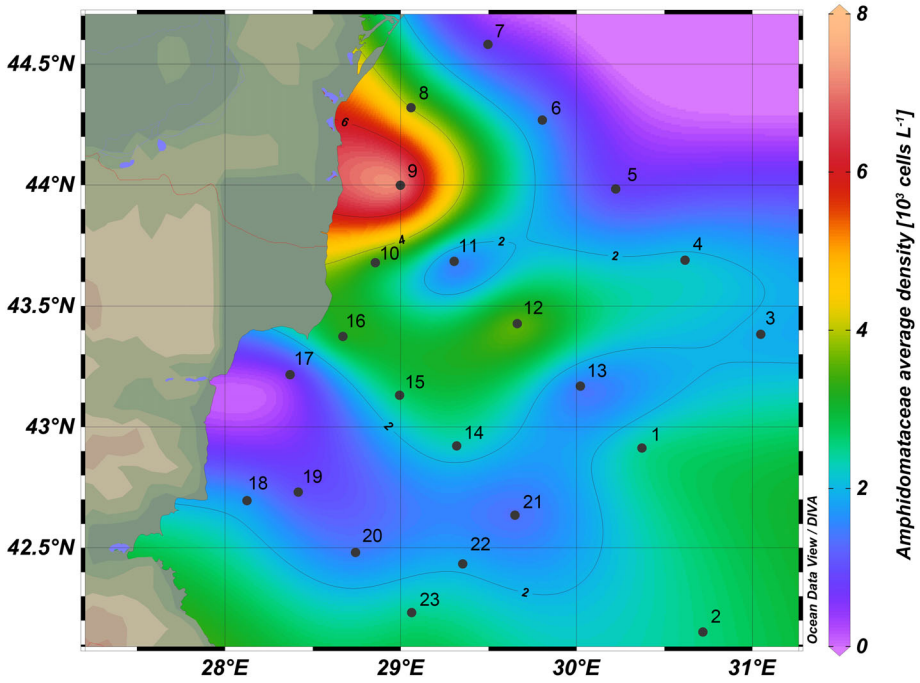

Figure 12. Distribution of average Amphidomataceae abundance (10^3 cells L^{-1}) along the Western Black Sea, from station 1 to 23. Thin lines in the figure represent contour lines of equal abundance, used to visualize the spatial distribution patterns across the sampled stations.

et al. 2012; Tillmann *et al*. 2014b) – can only be identified using electron microscopy. Therefore, in the quantitative analyses using fixed samples of the PHYCOB cruise, only a collective assessment of all Amphidomataceae within a single category is possible. Generally, in Lugol-fixed samples, it is difficult to differentiate *Azadinium* from similarly sized thecate species (e.g. *Heterocapsa* spp.), and confusion with small *Gymnodinium* species is also possible. Thus, the abundance data may to some extent overestimate the actual abundance of Amphidomataceae. However, the live observations on board provided a solid basis for reliably identifying and classifying cells as Amphidomataceae even in the fixed samples. This also raises important questions regarding historical underreporting: small Amphidomataceae were likely not quantified in previous studies due to their morphological resemblance to other small dinoflagellates and the limitations of light microscopy. It is now plausible that past counts of unidentified small thecate species, or even records attributed to *Heterocapsa* spp. or small *Gymnodinium*-like cells, may have in fact included Amphidomataceae. The patchy pattern observed in current distributions further suggests that previous underestimations may have stemmed from both spatial sampling gaps and taxonomic misclassification. These insights highlight the potential value of revisiting earlier datasets, where possible, with molecular or ultrastructural tools, in order to gain a clearer understanding of the historical presence and dynamics of this toxin-producing group.

With cell densities in the range of 10^2 to 10^4 cells L^{-1}, the abundance of Amphidomataceae in autumn 2021 was significant but not extraordinarily high. For comparisons, in terms of population density in the North Atlantic, peak densities around Ireland reached 8.3×10^4 cells L^{-1} and 4.7×10^6 cells L^{-1} for *Azadinium spinosum* and *Amphidoma languida*, respectively (Wietkamp *et al*. 2020; McGirr *et al*. 2022). Also, a bloom of *Am. languida* in the southern North Sea reached a maximum density of 1.2×10^5 cells L^{-1} (Wietkamp *et al*. 2020). In the Pacific, a bloom of *Azadinium polongum* Tillmann was detected in Peruvian coastal waters, with densities of up to 10^6 cells L^{-1} (Tillmann *et al*. 2017b). Recurrent dense blooms of Amphidomataceae are a well-documented phenomenon on the Argentine shelf in the South Atlantic, where bloom densities of $3–9 \times 10^6$ cells L^{-1} (Akselman & Negri 2012) or 2.8×10^5 cells L^{-1} (Tillmann *et al*. 2019) have been recorded. Notably, an exceptionally dense bloom almost exclusively made by amphidomatacean species of up to 3.2×10^7 cells L^{-1} occurred in 2021 (Guinder *et al*. 2024). Ecosystem and human health impact of such blooms, however, largely depend on the toxin production potential of the causative species. AZA production has only been confirmed for four of the 19 Amphidomataceae species that have been tested (Tillmann 2018a), and thus it is crucial to determine which species are present in any given occurrence of Amphidomataceae.

While light microscopic examinations of living and fixed samples indicate the presence of diverse species of Amphidomataceae in the area, it can provide only limited information about the occurring species. In contrast, electron microscopic observations of selected samples from the expedition provide evidence for the presence of several different species in the autumn plankton communities of the Black Sea. Without doubt, the newly described species *Am. pontica* (see discussion below) is also identified in the field samples. Moreover, SEM provides a record of the non-toxigenic species *Az. trinitatum*, which conform with the results of SSU based metabarcoding, indicating the presence of this species as reported by Dzhembekova *et al*. (2022). Based on the number of *Az. trinitatum* cells observed with SEM (Figs 9a–c and S2), this species is a quantitatively important component of the Amphidomataceae communities of the Black Sea. Cells identified here as *Az. trinitatum* conform with the original species

description (Tillmann *et al*. 2014a), including the observation that the antapical spine of the Black Sea specimens in many cases was poorly developed. Also, for the three strains analyzed in the species description paper, the presence of a distinct spine was predominant, but such structure was rudimentarily present or definitely missing in many cells (Tillmann *et al*. 2014a). *Azadinium trinitatum* is so far recorded from Iceland (Tillmann *et al*. 2014a), the Norwegian coast (Tillmann *et al*. 2018a), and Mutsu Bay, Japan (Takahashi *et al*. 2021), so the present record from the Black Sea indicate that this species is also capable to cope with lower salinity waters.

An unequivocal identification of *Az. spinosum* is more complicated. The presence of an antapical spine (albeit only rudimentary present for some specimens) and the position of the ventral pore on the left side in the middle of plate 1′ conform with the species description of *Az. spinosum* (Tillmann *et al*. 2009). However, a species provisionally described as *Az.* cf. *spinosum* was recently shown to conform in morphology with *Az. spinosum*, but in molecular phylogeny it is in a clade separated from *Az. spinosum*, and, importantly, all three tested strains lack AZA production (Tillmann *et al*. 2021). More local strains are thus needed to obtain long sequence information to evaluate the potential presence/absence of *Az. spinosum* and *Az.* cf. *spinosum* for the Black Sea. Nevertheless, a number of the field sample specimens conforming with *Az. spinosum* in terms of spine and ventral pore lack a rim around the apical pore plate (Fig. 9g–j), whereas for *Az.* cf. *spinosum* such a rim is always present (Tillmann *et al*. 2021). A lack of such a rim is a morphological trait characteristic for ribotype B strain of *Az. spinosum* (Tillmann *et al*. 2018a), which differs from *Az. spinosum* ribotype A strains also by the AZA toxin profile (Tillmann *et al*. 2018a, 2021). There is thus evidence that *Az. spinosum* ribotype B, whose presence up to now is known from Norway (Tillmann *et al*. 2018a), the North Sea (Tillmann *et al*. 2021), and the southwest Atlantic off Argentina (Tillmann *et al*. 2019), are also present in the Black Sea. For one cell of *Az. spinosum* appearance (including a rim around the pore plate) there was a deviating position of the ventral pore, which was located in a bulging leftward expansion of plate 1′ (Fig. 9j), but more material is needed to evaluate the species identity of such cells.

A number of cells of the PHYCOB field samples match the description of the species *Amphidoma languida* (Tillmann *et al*. 2012a), especially by the plate pattern and specific morphological features, particularly by the presence of only a single pore on both the pre- and postcingular plates. *Amphidoma languida* is an important species, as AZA production is found so far in all strains available from various areas of the ocean (Tillmann *et al*. 2012a, 2015, 2017a, 2021; Wietkamp *et al*. 2019a, 2020; Kuwata *et al*. 2024a). For a few specimens available in ventral view, a ventral depression at the tip of the anterior sulcal plate was visible. However, a new species very similar to *Am. languida*, *Am. fulgens*, was recently described, which is widely distributed in the Asian Pacific (Kuwata *et al*. 2024b). While there are significant sequence differences between *Am. languida* and *Am. fulgens*, accompanied with a lack of AZA production for *Am. fulgens*, both species largely share the same morphology (Kuwata *et al*. 2024b). Therefore, diagnostic features for distinguishing *Am. languida* from *Am. fulgens* remain somewhat unclear. The authors primarily cite the ventral depression, which is well-developed in *Am. fulgens* but either absent, rare, or weakly expressed in *Am. languida* (Kuwata *et al*. 2024b). However, a ventral depression is, although not explicitly noted for the type material (Tillmann *et al*. 2012a), reported for various other strains of *Am. languida* (Tillmann *et al*. 2015, 2017a; Wietkamp *et al*. 2019a), though not consistently present. Likewise, in *Am. fulgens*, there are strains where this feature is either absent or only weakly developed (Kuwata *et al*. 2024b). The application of species-specific qPCR primers specifically designed for Amphidomataceae (Smith *et al*. 2016) and for three of the toxic species (Toebe *et al*. 2013; Wietkamp *et al*. 2019b) in May 2019 in the northwestern Black Sea (Romanian and Bulgarian waters) confirmed the presence of Amphidomataceae in the area, but the targeted qPCR for the toxic species *Az. spinosum*, *Az. poporum*, and also for *Am. languida* were negative (Dzhembekova *et al*. 2022) suggesting that other amphidomatacean species were present. In contrast, NGS results indicated, albeit with very few sequences, the presence of *Am. languida* at three of the stations of this cruise (Dzhembekova *et al*. 2022). However, at the time of the analyses, the reference database included only sequences of *Am. languida*. The comparison between the V7-V9 region of the SSU rDNA sequences of *Am. languida*, *Am. fulgens*, and *Am. pontica* revealed 100% identical sequences between strains of the first two species, discussed in Kuwata *et al*. (2024b), and only a 1 bp mismatch with *Am. pontica*. Thus, the NGS sequences from this target region do not allow differentiation between *Am. languida*, *Am. fulgens*, and even the newly described species *Am. pontica*, since a difference of only 1 bp does not allow a robust species identification, and must be carefully interpreted. For future DNA metabarcoding-based studies focusing on amphidomatacean diversity, the application of other target regions may be more suitable (Liu *et al*. 2023). In addition, there are LSU-based qPCR primers specifically developed for *Am. languida* (Wietkamp *et al*. 2019b), but these were designed before *Am. fulgens* and *Am. pontica* were described. Testing these primers with an in silico PCR tool (https://primerdigital.com/tools/epcr.html) (Kalendar *et al*. 2024) indicate that for *Am. pontica* there is a high number of mismatches between the primers and the template, and that also for all but two strains of *Am. fulgens* whose sequences are available in GenBank no positive signals using these primers are expected. Therefore, the current *Am. languida* qPCR assay is still valuable to obtain data on presence and abundance of toxigenic *Am. languida* in field samples. To conclude, as is the case for *Az. spinosum* and *Az.* cf. *spinosum*, more information, including qPCR and ultimately strains, is needed for a final evaluation which other *Amphidoma* species, including *Am. languida* and/or *Am. fulgens*, are present in the Black Sea.

One cell observed in ventral view, referred to here as *Azadinium* sp. 1, exhibits such specific characteristics that it must be considered an as-yet undescribed species. Most notably, the position of the ventral pore (vp) is unique, located on the right side of a very broad plate 1′, in the middle of the suture between plates 1′ and 4′. There are other species of *Azadinium* where the vp is located right to the longitudinal cell axis, but for those the vp is on the suture of plate 1′ and 6″ for the much larger *Az. caudatum* var. *caudatum* (Nézan

et al. 2012) or in contact with the pores plate for *Az. dexteroporum* (Percopo *et al*. 2013), *Az. concinnum* (Tillmann *et al*. 2014a), *Az. luciferelloides* (Tillmann & Akselman 2016), *Az. zhuanum* Z.Luo, Tillmann & H.Gu (Luo *et al*. 2017), *Az. perforatum* Tillmann, Wietkamp & H.Gu (Tillmann *et al*. 2020), *Az. galwayense* R.Salas & Tillmann, and *Az. perfusorium* Tillmann & R.Salas (Salas *et al*. 2021). Another specimen available in dorsal view showing a relatively large and six-sided central epithecal intercalary plate (2a) might also represent *Azadinium* sp. 1, but for a full description of this taxon new material for more detailed analysis is required. Likewise, a single epitheca was recorded which conforms with the description of *Az. luciferelloides*, the species identified as causing dense blooms on the Argentinian shelf (Tillmann & Akselman 2016). This represents the first record of this species since its description, but more material from the Black Sea is required to ultimately confirm its presence. It is important to note that no cultured strains, and thus not sequence data (and data on toxin production), are available for this species yet, so metabarcoding data would not be able to confirm its presence. Finally, a few thecae were observed representing a yet undescribed dinophyte. This taxon clearly resembles *Amphidoma* in many aspects, i.e. the specific arrangement of the apical pore complex, the presence of six precingular plates, and the presence of a specific area with many small pores on one of the antapical plates, and the (likely) presence of a ventral depression. On the other hand, the taxon clearly has five apical plates and thus differ from other species of *Amphidoma*, which have six apical plates. There are distinct rows of pores on the relatively large apical plates, and with that the taxon resemble *Amphidoma alata* Tillmann, which however is larger, lacks an antapical field of pores, and has three narrow and three broad (i.e. six) apical plates (Tillmann 2018b). The taxon likely conforms with a cell designated as *Amphidoma* sp. 4 recorded from the 1991 bloom of the Argentine shelf (Tillmann 2018b). It will be interesting to find out if such dinophytes with five apical plates are closely related to *Amphidoma* or may represent another genus of Amphidomataceae.

Diagnosis of *Amphidoma pontica*

Our approach integrating detailed morphological analyses and molecular sequencing techniques provides conclusive evidence for the distinctiveness of *Am. pontica* sp. nov. The species without doubt is a new member of the genus *Amphidoma*, sharing the characteristic number of six plates each in the apical, precingular, cingular, and postcingular series characteristic for species of *Amphidoma* (Kofoid & Michener 1911; Balech 1971; Tillmann *et al*. 2012a), and also the peculiar morphology of the apical pore complex (presence of an X-plate with a characteristic finger-like extension connected to the cover plate) of Amphidomataceae (Tillmann *et al*. 2014c).

The type species of *Amphidoma* was widely considered to be *Am. nucula* F.Stein, but in fact, Loeblich and Loeblich III (1966) designated *Am. acuminata* F.Stein as the type of *Amphidoma*, despite Stein's doubts about the species (Stein 1883). A proposal that *Am. nucula*, whose morphology and plate pattern were much better described by Stein (1883), and also later by Dodge and Saunders (1985), should be a conserved type of *Amphidoma* (Tillmann & Gottschling 2018) was, however, rejected by the nomenclatural committee (Andersen 2020). In addition to the fact that the plate pattern of the type is thus poorly known, the diagnosis of the currently 14 accepted species of *Amphidoma* (Guiry 2025) is also partly challenging, as five species were described by Kofoid and Michener (1911) with some detailed verbal descriptions but unfortunately without illustrations. In any case, given the strong similarity of *Am. pontica* with *Am. languida* (see discussion below), we can follow the arguments and detailed discussion presented in Tillmann (2018b; table 2), which indicate that *Am. pontica* is clearly different in terms of size and shape from *Am. nucula*, *Am. acuminata*, *Am. steinii* J.Schiller, *Am. obtusa* Kofoid & Michener, *Am. elongata* Kofoid & Michener, *Am. depressa* Kofoid & Michener, *Am. curtata* Kofoid & Michener, and *Am. laticincta* Kofoid & Michener.

While the basic plate pattern (six apical, six precingular, and six postcingular plates) is the same in all *Amphidoma* species, additional details of the theca can be used for species diagnosis. Important features are the presence (or absence) and the position or distinct characteristics of three specific structures: the ventral pore (vp), the ventral depression (vd), and a potential specific modification of a part of the second antapical plate (2‴). In some species, this antapical plate features a distinctly separated antapical pore (ap), encircled by a raised ring (internally composed of multiple small pores), while others display only an undifferentiated field of small pores or no notable features at all. All these and other morphological criteria are summarized in Table 1 for a diagnostic discussion of the new species *Am. pontica* in comparison to *Amphidoma* species for which more recent electron microscopy studies are available.

Amphidoma pontica can be distinguished from *Am. trioculata* Tillmann, *Am. alata* Tillmann, and *Am. cyclops* Tillmann based on size; their size ranges do not overlap, although the lower and upper size limits of *Am. pontica* and these species come quite close. However, *Am. alata* is further differentiated by its distinct wing-like extensions (Tillmann 2018b). *Amphidoma cyclops* has a similarly large ventral depression compared to *Am. pontica*, but this species lacks an antapical pore (Tillmann 2018b). In many aspects, *Am. pontica* is similar to *Am. trioculata*. However, *Am. trioculata* is larger, has a noticeably rounder shape, and features numerous pores on the precingular plates (Tillmann 2018b).

Clearly, *Am. pontica* shares many similarities with two species: *Am. languida* (Tillmann *et al*. 2012a) and *Am. fulgens* (Kuwata *et al*. 2024b). They all have very similar size and cell shape, and also share the same characteristics in terms of the pyrenoid. While the swimming behaviour of *Am. fulgens* has not been specifically described (Kuwata *et al*. 2024b) both *Am. languida* (Tillmann *et al*. 2012a) and *Am. pontica* (Suppl. Video S1) also have the same way of movement. Consequently, these three species cannot be reliably distinguished under a light microscope. The morphological distinction between *Am. languida* and the newly described species *Am. fulgens* is particularly challenging and has been discussed in detail above with respect to the presence/absence of the ventral depression (vd). In *Am. pontica*, the vd is always present, although its size varies slightly. In the cells observed from field samples, the size of the vd appeared to be

Table 1. Morphological features of *Amphidoma pontica* sp. nov. and other selected small *Amphidoma* species.

Feature	*Am. pontica*	*Am. fulgens*	*Am. languida*	*Am. parvula*	*Am. trioculata*	*Am. alata*	*Am. cyclops*
Cell length	12.2–14.4	8.7–16.7	12.9 – 15.5	10.7–13.6	16.6 – 21.0	19.3 – 27.2	15.9 – 22.3
Cell width	9.4–11.9	7.5–14.0	9.7–14.1	9.6–12.9	16.1 – 20.4	17.0–23.0	14.3–20.7
Pyrenoid	One, episome	One, episome	One, episome	One, cingular plane	n.d.	n.d.	n.d.
Nucleus	Hyposome/center	Hyposome	Center	Center	n.d.	n.d.	n.d.
Pores on precingular plates	No	Yes, 1 per plate	Yes, 1 per plate	No	Yes, several per plate	No	Yes, few per plate
vp presence/position	Yes anterior right side of 1′	Yes anterior right side of 1′	Yes anterior right side of 1′	No	Yes anterior right side of 1′	No	n.d.[a]
vp size	0.22 µm	n.d.	0.24 µm	-	0.32 µm	-	-
vd presence/position	Yes anterior tip of sa	Yes anterior tip of sa	Yes/no[b] anterior tip of sa	Yes/no anterior tip of sa	Yes anterior tip of sa	No	Yes anterior tip of sa
vd size	0.45–0.71	0.17–0.5	0.20–0.27[c]	0.2[d]	0.36	-	0.78
ap	Yes	Yes	Yes	No[e]	Yes	No	No
Contact 6′ and 6″	No	Yes	Yes	Yes	Yes	Yes	Yes
Reference	This study	Kuwata *et al*. 2024b	Tillmann *et al*. 2012a	Tillmann *et al*. 2018b	Tillmann 2018b	Tillmann 2018b	Tillmann 2018b

Grey shading highlights the most important diagnostic features of *Am. pontica*. ap, antapical pore; n.d., not determined; vd, ventral depression; vp, ventral pore.
[a]For *Amphidoma cyclops* the anterior tip of plate 1′ was hidden and thus presence/absence of the vp for this species remain elusive.
[b]No vd was reported for the type strain SM2 (Tillmann *et al*. 2012a,b) but subsequently reported to be variably present in other strains of *Am. languida*.
[c]Measured from fig. 6I–M in Tillmann *et al*. (2017a).
[d]Measured from figs 33 and 34 in Tillmann *et al*. (2018a,b).
[e]Plate 2‴of *Am. parvula* has no antapical pore but a group of pores arranged in rows.

less variable, and individual cells with a vd diameter of 0.8–0.9 µm were observed among the field specimen but not in the cultured strains. This suggests that the expression of the vd may be influenced by culture conditions. It would thus be particularly interesting to examine field populations of *Am. languida* and *Am. fulgens* regarding the presence and development of the vd to better assess the significance of this feature for distinguishing between the two species.

The position of the nucleus in the cell is described as 'central' for *Am. languida* (Tillmann *et al*. 2012a) whereas for *Am. fulgens*, the nucleus is reported to be located in the hyposome (Kuwata *et al*. 2024b). In *Am. pontica*, the nucleus is found in the hyposome but has also been observed more centrally in the cingular region of the cell. However, since the position and even the shape of the dinoflagellate nucleus generally varies throughout the cell cycle (Tillmann & Elbrächter 2013), its exact location is likely not a reliable distinguishing morphological criterion.

Another feature initially suggested as useful for differentiating *Am. fulgens* from *Am. languida* is the presence of shiny refractile bodies at the posterior end of *Am. fulgens* cells (Kuwata *et al*. 2024b). However, at the time, these structures had not yet been examined in *Am. languida*, and shortly thereafter, similar refractile bodies—albeit smaller—were also detected in a Pacific strain of *Am. languida* (Kuwata *et al*. 2024a). Similar refractive structures are also present in *Am. pontica*. However, detailed ultrastructural studies using TEM are required for a more precise comparison with the findings in *Am. fulgens* and *Am. languida*.

The most significant diagnostic feature that clearly distinguishes *Am. pontica* from *Am. languida* and *Am. fulgens* is the consistent separation of plates 6″ and 6′ by the contact of plates 5″ and 1′. In all other *Amphidoma* species, plates 6″ and 6′ are in direct contact, and such a contact of the last apical and last precingular plate is also found for all species of *Azadinium* (Tillmann *et al*. 2012b, 2021; Kuwata *et al*. 2023).

Regarding the geographical distribution of these three very similar species—*Am. languida*, *Am. fulgens*, and *Am. pontica*—various records of *Am. languida* exist from the northern Atlantic to subarctic regions (Tillmann *et al*. 2012a, 2015; Wietkamp *et al*. 2019a), as well as from the South Atlantic (Argentina: Tillmann & Akselman 2016; Guinder *et al*. 2024) and the northern Pacific off the coast of Mexico (Kuwata *et al*. 2024a). *Amphidoma fulgens*, with strains found in Japan, Malaysia, and Vietnam, along with eDNA records from the Taiwan Strait, Bohai Sea, and East China Sea (Kuwata *et al*. 2024b), appears to be widely distributed across the Asian Pacific. With the now clearly defined morphology and sequence data for *Am. pontica*, further studies will determine whether this species has a broader distribution or is specific to the Black Sea, with a more limited geographic range.

ACKNOWLEDGMENTS

The authors thank Captain Tayfun Denizmen and R/V TÜBITAK MARMARA crew for their technical support and collaboration throughout the entire cruise. We greatly acknowledge technical support from Anne Müller (DNA extraction)

and Thomas Max (toxin analyses). Sampling was financed by EUROFLEETS+ under SEA-Call 'REGIONAL' funded from the EU H2020 Research and Innovation programme (GA 824077). We acknowledge support by the Open Access publication fund of Alfred-Wegener-Institut Helmholtz-Zentrum für Polar- und Meeresforschung. Open Access funding enabled and organized by Projekt DEAL.

AUTHOR CONTRIBUTIONS

Conceptualization: UT, ND. Investigation: UT, ND, OV, BK, FD. Writing: original draft: UT, ND. Writing: review and editing: all authors.

CONFLICT OF INTEREST

None of the authors have a conflict of interest to disclose.

DATA AVAILABILITY STATEMENT

The data that supports the findings of this study are available in the supplementary material of this article.

REFERENCES

Akoglu, E., Salihoglu, B., Libralato, S., Oguz, T. and Solidoro, C. 2014. An indicator-based evaluation of Black Sea food web dynamics during 1960–2000. *J. Mar. Syst.* **134**: 113–25.

Akselman, R. and Negri, R. M. 2012. Blooms of *Azadinium* cf. *spinosum* Elbrächter et Tillmann (Dinophyceae) in northern shelf waters of Argentina, southwestern Atlantic. *Harmful Algae* **19**: 30–8.

Andersen, R. A. 2020. Report of the nomenclature Committee for Algae: 22. *Taxon* **69**: 1099–101.

Bakan, G. and Büyükgüngör, H. 2000. The Black Sea. *Mar. Pollut. Bull.* **41**: 24–43.

Balech, E. 1971. Microplancton del Atlántico ecuatorial oeste (Equalant I). República Argentina, Armada Argentina Servico de Hidrografía Naval, Buenos Aires 654: 1–103.

Baytut, Ö., Moestrup, Ø., Lundholm, N. and Gönülol, A. 2013. Contributions to the diatom flora of the Black Sea from ultrastructural and molecular studies: new records of *Skeletonema marinoi, Pseudo-nitzschia pungens* var. *aveirensis* and *Chaetoceros tenuissimus* for the marine flora of Turkey. *Nova Hedwigia* **96**: 427–44.

Clark, K., Karsch-Mizrachi, I., Lipman, D. J., Ostell, J. and Sayers, E. W. 2016. GenBank. *Nucleic Acids Res.* **44**: 67–72.

Dodge, J. D. and Saunders, R. D. 1985. An SEM study of *Amphidoma nucula* (Dinophyceae) and description of the thecal plates in *A. Caudata*. *Arch. Protistenkd.* **129**: 89–99.

Dzhembekova, N., Moncheva, S., Slabakova, N. *et al.* 2022. New knowledge on distribution and abundance of toxic microalgal species and related toxins in the northwestern Black Sea. *Toxins* **14**: 685.

Dzhembekova, N., Urusizaki, S., Moncheva, S., Ivanova, P. and Nagai, S. 2017. Applicability of massively parallel sequencing on monitoring harmful algae at Varna Bay in the Black Sea. *Harmful Algae* **68**: 40–51.

Guinder, V. A., Tillmann, U., Rivarossa, M. *et al.* 2024. Extraordinary bloom of toxin-producing phytoplankton enhanced by strong retention in offshore continental shelf waters. *EGUsphere* . https://doi.org/10.5194/egusphere-2024-3157.

Guiry, M. D. 2025. Amphidoma. *In* Guiry, M. D. and Guiry, G. M. (Eds). *AlgaeBase. World-Wide Electronic Publication*. National University of Ireland Galway (taxonomic information republished from AlgaeBase with permission of M.D. Guiry). Accessed through: World Register of Marine Species at http://www.marinespecies.org/aphia.php?p=taxdetails&id=109517. searched on 2025-04-05.

Kalendar, R., Otarbay, Z. and Ismailova, A. 2024. In silico PCR analysis: a comprehensive bioinformatics tool for enhancing nucleic acid amplification assays. *Front. Bioinform.* **4**: 1464197.

Katoh, K., Rozewicki, J. and Yamada, K. D. 2019. MAFFT online service: multiple sequence alignment, interactive sequence choice and visualization. *Brief. Bioinform.* **20**: 1160–6.

Keller, M. D., Selvin, R. C., Claus, W. and Guillard, R. R. L. 1987. Media for the culture of oceanic ultraphytoplankton. *J. Phycol.* **23**: 633–8.

Kideys, A. E. 2002. Fall and rise of the Black Sea ecosystem. *Science* **297**: 1482–4.

Kisselew, I. A. 1950. *Dinoflagellata*. Fauna URSS, Moscova, Russia.

Kofoid, C. A. and Michener, J. R. 1911. Reports on the scientific results of the expedition to the eastern tropical Pacific, in charge of Alexander Agassiz, by the U.S. fish commission steamer ALBATROSS, from October 1904, to march, 1906, Lieut. L.M. Garrett, U.S.N., commanding. XXII. New genera and species of dinoflagellates. *Bull. Mus. Comp. Zool.* **54**: 267–302.

Krakhmalny, A. F., Okolodkov, J. B., Bryantseva, Y. *et al.* 2018. Revision of the dinoflagellate species composition of the Black Sea. *Algologia* **28**: 428–48.

Krock, B., Tillmann, U., Tebben, J., Trefaults, N. and Gu, H. 2019. Two novel azaspiracids from *Azadinium poporum*, and a comprehensive compilation of azaspiracids produced by Amphidomataceae (Dinophyceae). *Harmful Algae* **82**: 1–8.

Kumar, S., Stecher, G., Li, M. and Knyaz, C. 2018. Mega X: molecular evolutionary genetics analysis across computing platforms. *Mol. Biol. Evol.* **35**: 1547–9.

Kumar, S., Stecher, G., Suleski, M., Sanderford, M., Sharma, S. and Tamura, K. 2024. MEGA12: molecular evolutionary genetic analysis version 12 for adaptive and green computing. *Mol. Biol. Evol.* **41**: 1–9.

Kuwata, K., Hernández-Becerril, D. U., Ozawa, M. *et al.* 2024a. First report of toxigenic *Amphidoma languida* (Amphidomataceae, Dinophyceae) from the Pacific, with reference to intracellular ultrastructure and azaspiracid compounds. *Phycol. Res.* **72**: 266–78.

Kuwata, K., Lum, W. M., Takahashi, K. *et al.* 2024b. Phylogeny and ultrastructure of a non-toxigenic dinoflagellate *Amphidoma fulgens* sp. nov. (Amphidomataceae, Dinophyceae), with a wide distribution across Asian Pacific. *Harmful Algae* **138**: 102701.

Kuwata, K., Lum, W. M., Takahashi, K. *et al.* 2023. A new small thecate dinoflagellate *Azadinium anteroporum* sp. nov. (Amphidomataceae, Dinophyceae) isolated from the Asian Pacific. *Phycologia* **62**: 303–14.

Liu, M., Tillmann, U., Ding, G., Wang, A. and Gu, H. 2023. Metabarcoding revealed a high diversity of Amphidomataceae (Dinophyceae) and the seasonal distribution of their toxigenic species in the Taiwan Strait. *Harmful Algae* **124**: 102404.

Loeblich, A. R. J. and Loeblich, A. R. III 1966. Index to the genera, subgenera, and sections of the Pyrrhophyta. *Stud. Trop. Oceanogr.* **3**: 1–94.

Luo, Z., Gu, H., Krock, B. and Tillmann, U. 2013. *Azadinium dalianense*, a new dinoflagellate from the Yellow Sea, China. *Phycologia* **52**: 625–36.

Luo, Z., Krock, B., Mertens, K. *et al.* 2017. Adding new pieces to the *Azadinium* (Dinophyceae) diversity and biogeography puzzle: non-toxigenic *Azadinium zhuanum* sp. nov. from China, toxigenic *A. Poporum* from the Mediterranean, and a non-toxigenic *A. Dalianense* from the French Atlantic. *Harmful Algae* **66**: 65–78.

McGirr, S., Clark, D., Kilkoyne, J., Silke, J. and Touzet, N. 2022. Co-localisation of Azaspiracid analogs with the dinoflagellate species *Azadinium spinosum* and *Amphidoma languida* in the southwest of Ireland. *Microb. Ecol.* **83**: 635–46.

Moncheva, S., Boicenco, L., Mikaelyan, A. *et al*. 2019. 1.3.2 Phytoplankton. *In* Krutov, A. (Ed.). *State of the Environment of the Black Sea (2009–2014/5)*. Publications of the Commission on the Protection of the Black Sea Against Pollution (BSC, Istanbul), Turkey, pp. 225–85.

Moncheva, S., Doncheva, V., Boicenco, L., Sahin, F., Slabakova, N. and Culcea, O. 2014. Report on the MISIS cruise intercalibration exercise: Phytoplankton. Ex. Ponto, Constanta, Romania.

Moncheva, S., Gotsis-Skretas, O., Pagou, K. and Krastev, A. 2001. Phytoplankton blooms in Black Sea and Mediterranean coastal ecosystems subjected to anthropogenic eutrophication: similarities and differences. *Estuar. Coast. Shelf Sci.* **53**: 281–95.

Moncheva, S. and Parr, B. 2010. *Manual for Phytoplankton Sampling and ANalysis in the Black Sea*. Black Sea Commission, Istanbul, Turkey.

Nei, M. and Kumar, S. 2000. *Molecular Evolution and Phylogenetics*. Oxford University Press, New York.

Nesterova, D., Moncheva, S., Mikaelyan, A. *et al*. 2008. Chapter 5. The state of phytoplankton. *In* Oguz, T. (Ed.). *State of the Environment of the Black Sea (2001–2006/7)*. Black Sea Commission Publications 2008–3, Istanbul, Turkey, pp. 133–67.

Nézan, E., Tillmann, U., Bilien, G. *et al*. 2012. Taxonomic revision of the dinoflagellate *Amphidoma caudata*: transfer to the genus *Azadinium* (Dinophyceae) and proposal of two varieties, based on morphological and molecular phylogenetic analyses. *J. Phycol.* **48**: 925–39.

Nylander, J. A. A. 2004. MrModeltest v2. Program distributed by the author. Evolutionary Biology Centre, Uppsala University.

Percopo, I., Siano, R., Rossi, R., Soprano, V., Sarno, D. and Zingone, A. 2013. A new potentially toxic *Azadinium* species (Dinophyceae) from the Mediterranean Sea, *A. Dexteroporum* sp. nov. *J. Phycol.* **49**: 950–66.

Peteva, Z., Krock, B., Georgieva, S., Stancheva, M. and Max, T. 2023. Food safety status of mussels from Bulgarian coast in regard of marine biotoxins. *Bulg. J. Agric. Sci.* **29**: 536–43.

Ronquist, F., Teslenko, M., van der Mark, P. *et al*. 2012. MrBayes 3.2: efficient Bayesian phylogenetic inference and model choice across a large model space. *Syst. Biol.* **61**: 539–42.

Ryabushko, L. I. 2003a. *Atlas of Toxic Microalgae of the Black Sea and the Sea of Azov*. Ministry of Defense of Ukraine, National Academy of Sciences of Ukraine, Scientific Center of Armed Forces of Ukraine, Sevastopol, Ukraine.

Ryabushko, L. I. 2003b. *Potentially Harmful Microalgae of the Azov and Black Sea Basin*. Institute of Biology of the Southern Seas, National Academy of Sciences of the Ukraine, Sevastopol: ECOSI-Gidrofizica.

Salas, R., Tillmann, U., Gu, H., Wietkamp, S., Krock, B. and Clarke, D. 2021. Morphological and molecular characterization of multiple new *Azadinium* strains revealed a high diversity of non-toxigenic species of Amphidomataceae (Dinophyceae) including two new *Azadinium* species in Irish waters, North East Atlantic. *Phycol. Res.* **69**: 88–115.

Salas, R., Tillmann, U., John, U. *et al*. 2011. The role of *Azadinium spinosum* (Dinophyceae) in the production of azaspiracid shellfish poisoning in mussels. *Harmful Algae* **10**: 774–83.

Sato, S., Nishimura, T., Uehara, K. *et al*. 2011. Phylogeography of *Ostreopsis* along west Pacific coast, with special reference to a novel clade from Japan. *PLoS One* **6**: e27983.

Schiller, J. 1937. Dinoflagellatae (Peridineae) in monographischer Behandlung. *In* Rabenhorst, L. (Ed.). *Dr. L. Rabenhorst's Kryptogamen-Flora von Deutschland, Österreich und der Schweiz*. Johnson, New York, pp. 1–590.

Schlitzer, R. 2023. Ocean Data View. Available from: https://odv.awi.de.

Scholin, C. A., Herzog, M., Sogin, M. and Anderson, D. M. 1994. Identification of group- and strain-specific genetic markers for globally distributed *Alexandrium* (Dinophyceae). II. Sequence analysis of a fragment of the LSU rRNA gene. *J. Phycol.* **30**: 999–1011.

Smith, K. F., Rhodes, L., Harwood, D. T. *et al*. 2016. Detection of *Azadinium poporum* in New Zealand: the use of molecular tools to assist with species isolations. *J. Appl. Phycol.* **28**: 1125–32.

Stein, F. 1883. *Der Organismus der Infusionsthiere nach eigenen Forschungen in systematischer Reihenfolge bearbeitet*. W. Engelmann, Leipzig.

Takahashi, K., Lum, W. M., Benico, G. *et al*. 2021. Toxigenic strains of *Azadinium poporum* (Amphidomataceae, Dinophyceae) from Japan and Vietnam, with first reports of *A. Poporum* (ribotype A) and *A. Trinitatum* in Asian Pacific. *Phycol. Res.* **69**: 175–87.

Tillmann, U. 2018a. Amphidomataceae. *In* Shumway, S. E., Burkholder, J. A. and Morton, S. L. (Eds). *Harmful Algae Blooms, a Compendium Desk Reference*. Wiley, Hoboken, pp. 575–82.

Tillmann, U. 2018b. Electron microscopy of a 1991 spring plankton sample from the Argentinean shelf reveals the presence of four new species of Amphidomataceae (Dinophyceae). *Phycol. Res.* **66**: 269–90.

Tillmann, U. and Akselman, R. 2016. Revisiting the 1991 algal bloom in shelf waters off Argentina: *Azadinium luciferelloides* sp. nov. (Amphidomataceae, Dinophyceae) as the causative species in a diverse community of other amphidomataceans. *Phycol. Res.* **64**: 160–75.

Tillmann, U., Edvardsen, B., Krock, B., Smith, K. F., Paterson, R. F. and Voß, D. 2018a. Diversity, distribution, and azaspiracids of Amphidomataceae (Dinophyceae) along the Norwegian coast. *Harmful Algae* **80**: 15–34.

Tillmann, U. and Elbrächter, M. 2013. Cell division in *Azadinium spinosum* (Dinophyceae). *Bot. Mar.* **56**: 399–408.

Tillmann, U., Elbrächter, M., John, U. and Krock, B. 2011. A new non-toxic species in the dinoflagellate genus *Azadinium*: *A. Poporum* sp. nov. *Eur. J. Phycol.* **46**: 74–87.

Tillmann, U., Elbrächter, M., John, U., Krock, B. and Cembella, A. 2010. *Azadinium obesum* (Dinophyceae), a new nontoxic species in the genus that can produce azaspiracid toxins. *Phycologia* **49**: 169–82.

Tillmann, U., Elbrächter, M., Krock, B., John, U. and Cembella, A. 2009. *Azadinium spinosum* gen. Et sp. nov. (Dinophyceae) identified as a primary producer of azaspiracid toxins. *Eur. J. Phycol.* **44**: 63–79.

Tillmann, U. and Gottschling, M. 2018. Proposal to conserve the name *Amphidoma* (Dinophyceae) as being feminine and with a conserved type. *Taxon* **67**: 13.

Tillmann, U., Gottschling, M., Guinder, V. and Krock, B. 2018b. *Amphidoma parvula* (Amphidomataceae), a new planktonic dinophyte from the Argentine sea. *Eur. J. Phycol.* **53**: 14–28.

Tillmann, U., Gottschling, M., Krock, B., Smith, K. F. and Guinder, V. 2019. High abundance of Amphidomataceae (Dinophyceae) during the 2015 spring bloom of the Argentinean shelf and a new, non-toxigenic ribotype of *Azadinium spinosum*. *Harmful Algae* **84**: 244–60.

Tillmann, U., Gottschling, M., Nézan, E. and Krock, B. 2015. First record of *Azadinium dexteroporum* and *Amphidoma languida* (Amphidomataceae, Dinophyceae) from the Irminger Sea off Iceland. *Mar. Biodivers. Rec.* **8**: 1–11.

Tillmann, U., Gottschling, M., Nézan, E., Krock, B. and Bilien, G. 2014a. Morphological and molecular characterization of three new *Azadinium* species (Amphidomataceae, Dinophyceae) from the Irminger Sea. *Protist* **165**: 417–44.

Tillmann, U., Jaen, D., Fernández, L. *et al*. 2017a. *Amphidoma languida* (Amphidomataceae, Dinophyceae) with a novel azaspiracid toxin profile identified as the cause of molluscan contamination at the Atlantic coast of southern Spain. *Harmful Algae* **62**: 113–26.

Tillmann, U., Krock, B. and Taylor, B. 2014b. *Azadinium caudatum* var. *margalefii*, a poorly known member of the toxigenic genus *Azadinium* (Dinophyceae). *Mar. Biol. Res.* **10**: 941–56.

Tillmann, U., Salas, R., Gottschling, M., Krock, B., O'Driscoll, D. and Elbrächter, M. 2012a. *Amphidoma languida* sp. nov. (Dinophyceae) reveals a close relationship between *Amphidoma* and *Azadinium*. *Protist* **163**: 701–19.

Tillmann, U., Salas, R., Jauffrais, T., Hess, P. and Silke, J. 2014c. AZA: the producing organisms – biology and trophic transfer. *In* Botana, L. M. (Ed.). *Seafood and Freshwater Toxins*. CRC Press, Boca Raton, USA, pp. 773–98.

Tillmann, U., Sánchez Ramírez, S., Krock, B. and Bernales Jiménez, A. 2017b. A bloom of *Azadinium polongum* in coastal waters off Peru. *Rev. Biol. Mar. Oceanogr.* **52**: 591–610.

Tillmann, U., Söhner, S., Nézan, E. and Krock, B. 2012b. First record of *Azadinium* from the Shetland Islands including the description of *A. Polongum* sp. nov. *Harmful Algae* **20**: 142–55.

Tillmann, U., Wietkamp, S., Gu, H., Krock, B., Salas, R. and Clarke, D. 2021. Multiple strains of Azadinium spinosum reveal diverse but stable toxin profiles, and a new nontoxigenic *Az.* cf. *spinosum*. *Microorganisms* **9**: 134.

Tillmann, U., Wietkamp, S., Krock, B., Tillmann, A., Voss, D. and Gu, H. 2020. Amphidomataceae (Dinophyceae) in the western Greenland area, including the description of *Azadinium perforatum* sp. nov. *Phycologia* **59**: 63–88.

Toebe, K., Joshi, A. R., Messtorff, P., Tillmann, U., Cembella, A. and John, U. 2013. Molecular discrimination of taxa within the dinoflagellate genus *Azadinium*, the source of azaspiracid toxins. *J. Plankton Res.* **35**: 225–30.

Tomas, C. R. (Ed.). 1997. *Identifying Marine Phytoplankton*. Academic Press, San Diego.

Twiner, M. J., Rehmann, N., Hess, P. and Doucette, G. J. 2008. Azaspiracid shellfish poisoning: A review on the chemistry, ecology, and toxicology with emphasis on human health impacts. *Mar. Drugs* **6**: 39–72.

Wietkamp, S., Krock, B., Clarke, D. *et al*. 2020. Distribution and abundance of azaspiracid-producing dinophyte species and their toxins in North Atlantic and North Sea waters in summer 2018. *PLoS One* **15**: e0235015.

Wietkamp, S., Krock, B., Gu, H., Voß, D., Klemm, K. and Tillmann, U. 2019a. Occurrence and distribution of Amphidomataceae (Dinophyceae) in Danish coastal waters of the North Sea, the Limfjord, and the Kattegat/belt area. *Harmful Algae* **88**: 101637.

Wietkamp, S., Tillmann, U., Clarke, D. and Toebe, K. 2019b. Molecular detection and quantification of the toxigenic dinoflagellate *Amphidoma languida* (Amphidomataceae, Dinophyceae). *J. Plankton Res.* **41**: 101–13.

Zaitsev, Y. and Mamaev, V. 1997. *Biological Diversity in the Black Sea: A Study of Change and Decline*. United Nations Publishing, New York, USA.

Zaitsev, Y. P. 1992. Recent changes in the trophic structure of the Black Sea. *Fish. Oceanogr.* **1**: 180–9.

Zhang, Y., Pavlovska, M., Stoica, E. *et al*. 2020. Holistic pelagic biodiversity monitoring of the Black Sea via eDNA metabarcoding approach: from bacteria to marine mammals. *Environ. Int.* **135**: 105307.

SUPPORTING INFORMATION

Additional Supporting Information may be found in the online version of this article at the publisher's web-site:

Table S1. Investigated azaspiracids including associated quantification and qualification transitions. Compounds marked with a '?' are preliminarily observed before but have not yet been fully characterized.

Table S2. Information on Amphidomataceae strains used for phylogenetic analyses, including original species designations, strain codes, geographic origins, and GenBank accession numbers.

Table S3. Genetic pairwise p-distances between *Amphidoma* species, based on ITS sequences (16 sequences, 639 positions).

Table S4. Genetic pairwise p-distances between *Amphidoma* species, based on partial LSU rDNA sequences (16 sequences, 779 positions).

Table S5. Genetic pairwise p-distances between *Amphidoma* species, based on partial SSU rDNA sequences (16 sequences, 779 positions).

Figure S1. *Amphidoma pontica* (strain BS 6-F9) SEM of different cells showing deviating plate pattern of epithecal (a–e) or hypothecal (e, f) plates. (a) A cell with 5 apical plates, interpreted here as a fusion of plates 2′ and 3′. (b–d) Cells with 7 apical plates, interpreted here as subdivision (indicated by α and β) of certain apical plates. (e) A cell with 5 postcingular plates, interpreted here as a fusion of plates 2‴ and 3‴. (f) A cell with 7 precingular plates, interpreted here as subdivision (indicated by α and β) of plate 3‴. Scale bars: 2 μm.

Figure S2. SEM of *Azadinium trinitatum* cells observed in the Black Sea field sample. (a–g) Cells in ventral (a–d) and dorsal (e–g) view. (h–j) Epithecal plates in apical view. (k) Detailed ventral view of the apical pore complex. (l) Epithecal plates in left-lateral view. Scale bars: 2 μm (a–j, l) or 1 μm (k).

Figure S3. SEM of *Azadinium* and *Amphidoma* sp. cells observed in the Black Sea field sample. (a, b) *Azadinium* cf. *spinosum*, cells in apical view (a), or epitheca in ventral view (b). (c–f) *Amphidoma languida* (c) Cell in dorsal view. (d–f) Epitheca in apical view. (g–n) Cells of a yet undetermined *Amphidoma* sp. 1. (k) Apical view showing epithecal plates. (g–l) Cells in dorsal view. (m, n) Cell in dorsal/apical view. Scale bars: 2 μm.

Video S1 *Amphidoma pontica*, light microscopy of living cells.